

---

# OmniArch: Building the Foundation Model for Scientific Computing

---

**Tianyu Chen**  
Beihang University  
tianyuc@buaa.edu.cn

**Haoyi Zhou**  
Beihang University  
haoyi@buaa.edu.cn

**Ying Li**  
Peking University  
myendless@stu.pku.edu.cn

**Hao Wang**  
Peking University  
haowang@stu.pku.edu.cn

**Chonghan Gao**  
Beihang University  
gaoch@buaa.edu.cn

**Rongye Shi**  
Beihang University  
shirongye@buaa.edu.cn

**Shanghang Zhang**  
Peking University  
shanghang@pku.edu.cn

**Jianxin Li**  
Beihang University  
lijx@buaa.edu.cn

## Abstract

Foundation models have revolutionized language modeling, while whether this success is replicated in scientific computing remains unexplored. We present OmniArch, the first prototype aiming at solving multi-scale and multi-physics scientific computing problems with physical alignment. We addressed all three challenges with one unified architecture. Its pre-training stage contains a Fourier Encoder-decoder fading out the disharmony across separated dimensions and a Transformer backbone integrating quantities through temporal dynamics, and the novel PDE-Aligner performs physics-informed fine-tuning under flexible conditions. As far as we know, we first conduct 1D-2D-3D united pre-training on the PDEBench, and it sets not only new performance benchmarks for 1D, 2D, and 3D PDEs but also demonstrates exceptional adaptability to new physics via in-context and zero-shot learning approaches, which supports realistic engineering applications and foresight physics discovery.

## 1 Introduction

Developing robust neural surrogate models for temporal partial differential equations (PDEs) is crucial for various scientific and engineering applications, including aircraft design, weather forecasting, and semiconductor manufacturing [1, 21]. These PDEs describe spatial-temporal dynamic systems that are foundational to these industries. Traditional scientific computing methods, such as Finite Element Methods (FEMs) and Finite Volume Methods (FVMs) [20], require extensive handcrafted coding and are computationally intensive, even on state-of-the-art High-Performance Computing (HPC) clusters. To expedite PDE solving, pioneers have explored the construction of neural operators that learn mappings between function spaces, offering the potential to generalize across different discretizations. For the requisite precision, neural operators are often enhanced with physics-informed normalization techniques, such as customized loss functions derived from the governing physical equations [26].

The primary limitation of neural operator methods lies in their case-specific design, restricting their application scope and hindering broad transferability across diverse physical systems. Recent efforts aim to enhance the transferability of neural operators by developing foundational models that leverage advancements in learning strategies, architectural design, and data curation. In terms of learning, the

*pre-train and fine-tune* paradigm, proven effective for Fourier Neural Operator (FNO) models [32], has been adapted to PDE contexts. Additionally, Lie group-based self-supervised learning (Lie-SSL) [18] introduces physics-constrained transformations for PDEs, primarily addressing inverse problems. Architecturally, innovations like ICON\_LM [38], and PITT [14] incorporate language model principles to enhance neural operator learning, enabling generalization through equation captions. The Factformer [11] introduces a scalable transformer for multi-dimensional PDE data, with the Multi-Physics Pre-training (MPP) [17] further extending this approach to 2D data pre-training. From a data-centric viewpoint, resources such as PDEBench [34] and PDEArena [8] offer well-structured datasets that facilitate pre-training and the establishment of rigorous benchmarks.

While attempting unified learning of multiple PDE solvers in a single model, multi-scale and multi-physics challenges persist. The above surrogate models, often constrained by the fixed mapping grid (MPP, Lie-SSL, ICON\_LM) and single-time step observation window (MPP, Facyformer, PITT), struggle with flexible spatial grid input and long-sequence roll-out predictions.

In this work, we study how to frame the foundation model learning paradigms for Scientific Computing tasks w.r.t PDEs, namely OmniArch. For the pre-training stage, we define a flexible pipeline to deal with multiple-physics spatio-temporal data and convert the forward problem learning into popular auto-regressive tasks that can be scaled up easily. For the pre-training stage, we devise a flexible pipeline to handle multi-physics spatio-temporal data and reformulate the forward problem as scalable autoregressive tasks. Specifically, we employ a Fourier encoder to convert coordinate and observation data into frequency components (modes). We use truncated modes to form PDE token embeddings, sequenced for processing by transformer blocks, and we design the PDE-Aligner during fine-tuning to align predictions with known physical laws and principles, improving the model concordance to conventional physical constraints.

We release our models' base and large variants<sup>1</sup>, concurrently addressing 1D, 2D, and 3D PDEs. Evaluating performance across 11 PDE types from PDEBench and PDEArena, our OmniArch achieves state-of-the-art results, as illustrated in Figure 1. For the Computational fluid dynamics (CFD) related tasks, we observe one to two orders of magnitude reductions in normalized root mean squared error. Moreover, our models exhibit emergent capabilities, such as zero-shot generalization to novel PDE systems and in-context learning of neural operators. The representations learned by OmniArch demonstrate versatility, readily adaptable to inverse problems. Notably, OmniArch facilitates multi-scale inference, accommodating a range of input grid resolutions with moderate precision trade-offs. In summary, our key contributions and findings include:

- We introduce OmniArch, the first foundation model to successfully conduct 1D-2D-3D united pre-training. Using a Fourier Encoder-decoder, OmniArch allows for flexible grid inputs, enabling unified multi-scale training. The Temporal Mask effectively addresses inconsistencies in multi-physics systems, allowing different physical quantities and time steps to be learned simultaneously within a shared Transformer backbone.
- We develop the PDE-Aligner for physics-informed fine-tuning, which leverages hidden representations of equations and other physical priors to align with observed physical field dynamics.
- After fine-tuning, OmniArch achieves state-of-the-art performance on 11 types of PDEs from the PDEBench and PDEArena benchmarks. The model exhibits in-context learning capabilities and demonstrates promising zero-shot performance.

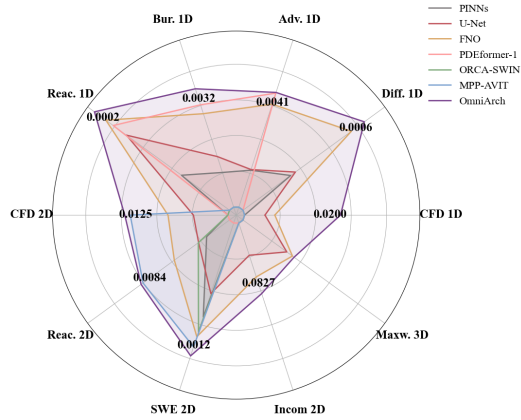


Figure 1: OmniArch achieves state-of-the-art performance (nRMSE Loss) on a broad range of tasks. The baselines include the task-specific expert models [26, 29, 12] and the pre-trained models [17, 39, 13].

<sup>1</sup><https://openi.pcl.ac.cn/cty315/OmniArch>

## 2 Related Works

**Learned PDE Solvers.** Deep Learning for solving PDEs has been a recent focal point of research [16, 9], including physics-informed methods [26], GNN-based techniques [36, 22], and neural operator models like DeepONet [15] and FNO [12]. While effective, these models often require task-specific training and struggle with generalization. ICON\_LM [37], MPP [17], PDEformer-1 [39] aim to generalize across diverse physical systems but limit to a single dimension.

**Foundation Models.** The Foundation Models [6, 3, 25, 24, 35, 23] have emerged as pivotal elements in the field of natural language processing, computer vision, and cross-modal tasks. After large-scale pre-trained with the transformer backbone, they serve as the bedrock for a multitude of downstream tasks by fine-tuning [41] or in-context learning [10]. Recently, they have shown promise in scientific fields, exemplified by FourcastNet [21] for weather forecasting, OpenLAM [40] for chemistry, and HyenaDNA [19] for biomedical tasks. However, applying foundation models to scientific computing, particularly PDE solving, remains an emerging and pioneering area.

## 3 Method

The foundation models [6, 3, 25, 24, 35, 23] have shown significant success with broad generation to various inputs and downstream tasks. Building a similar model for scientific computing should require addressing dynamic and complex physical systems and learning intrinsic laws from wild physical phenomena. We highlight the major challenges as three-fold:

**Multi-Scale** The ability to handle inputs of different dimensions (1D, 2D, 3D), varying grid resolutions, and diverse grid shapes. For example, fluid dynamics simulations can range from simple one-dimensional pipe flow to complex three-dimensional turbulent flow, and the model must maintain accuracy and consistency across these different scales.

**Multi-Physics** The capability to handle dynamic systems involving different physical quantities. For instance, in meteorology, multiple physical quantities such as wind speed, temperature, and humidity interact, requiring the model to process these different physical fields simultaneously.

**Physical Alignment** Allowing flexible incorporation of physical priors such as governing equations, symmetries, conservation laws, and boundary conditions into the solution process. For example, in heat conduction problems, the law of conservation of energy and boundary conditions is crucial for predicting temperature distributions.

The proposed OmniArch Model follows the predominant *pre-training-then-fine-tune* paradigm. In subsection 3.1, we utilize Fourier Encoders and Decoders to address the multi-scale challenge and employ the Temporal Attention mechanism to handle multi-physics generalization problems. In subsection 3.2, we leverage the PDE-Aligner in the fine-tuning stage, allowing the incorporation of physical priors in textual form into the model’s learning and adaptation process.

### 3.1 Pre-training OmniArch: Flexibly Learning from Different Dynamic Systems

The overall pre-training framework of OmniArch is illustrated in Figure 2. For physical data of different dimensions (1D, 2D, 3D), we use separate Fourier Encoders to transform their coordinates and observed physical field values into the frequency domain. High and low frequencies are truncated in the frequency domain so that data from different grids have the same length of embedded representations. Then, these representations are processed through shared Transformer modules to model the integral operators along the time axis. We leverage the Temporal Mask to ensure that each physical quantity can simultaneously attend to all physical quantities and previous time steps. Finally, the predicted embedding representations are used to recover the predicted frequency domain signals. We involve zero-padding to keep these signals with the target physical field shape and perform individual inverse Fourier transforms to output the corresponding physical field predictions.

#### 3.1.1 Encoder/Decoder in Fourier Domain

The multi-scale challenge needs proper representation of inputs from different dimensions, varying grid resolutions, and shapes. Inspired by the Fourier transforms [2] convert the sequential signals into frequency components, we re-organize the multi-scale inputs in the spatial domain into the

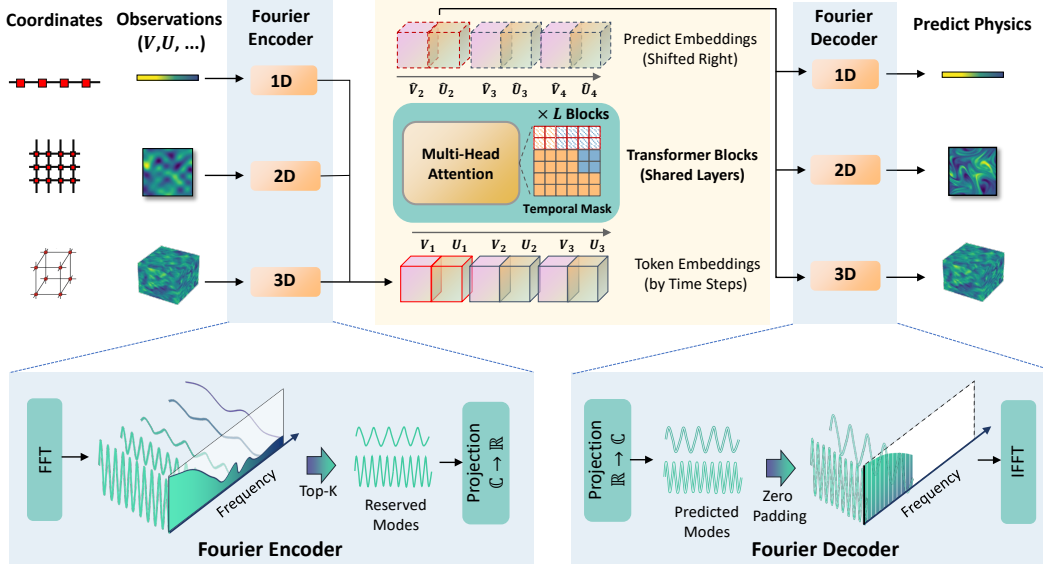


Figure 2: **The overview of OmniArch.** The *Fourier Encoder* converts coordinates and physical fields into frequency domains, enabling unified training for 1D, 2D, and 3D data. Reserved frequency modes form PDE token embeddings for *Shared Transformer Blocks*. Tokens are grouped by timestep to create a *Temporal Mask* for prediction. Predicted modes are decoded using IFFT with zero padding to recover the physical field.

multi-component ones in the frequency domain. The traditional pipeline includes convolutional encoders [27], which capture the local features in separated dimensions while the global information exchange happens at the channels' explicit mixing. The results of Fourier transforms are complex coefficients that measure the magnitude and phase of decomposed periodic components and the global information is naturally weighted, which also applies to the complex boundary conditions and heterogeneous grids. Based on that, we further introduce the filter-like components selecting mechanism that distinguishes the high-frequency (detailed variations) and low-frequency (overall trends) ones in physical inputs, which may maintain different patterns and distribution ratios among the local and global representation. Thus, we can build a universal representation with different resolutions and grid shapes in one flexible network architecture.

From a computing-efficient perspective, the forward procedure of Fourier Encoders can be implemented through the Fast Fourier Transform (FFT) with the  $O(N \log N)$  complexity while the convolution operation ends in  $O(N^2)$ . The sparsity and separability of frequency domain features facilitate the subsequent Transformer modules in efficiently processing temporal information, reducing the model's parameters and computational overhead for better training and inference efficiency.

Let  $\mathcal{U} \in \mathbb{R}^{T \times D \times 1}$  stand for the physical field inputs. If we have a real-valued input  $u(x^{(d)}, t) \in \mathbb{R}$  from  $d$ -th index and  $t$ -th time step, the Fourier Encoder firstly applies FFT to convert it from the spatial domain to the frequency domain. Note that  $D$  is the total dimension and  $d$  denotes the sequential index (1, 2, 3 . . .), for example,  $D = D_1 + D_2 + D_3 = 6$  for 1D, 2D and 3D inputs. Then we have the frequency domain representation  $\hat{\mathcal{U}} \in \mathbb{C}^{T \times F \times 1}$  after traversing through all time steps and dimensions. As previously discussed, we design a filter-like mechanism by applying the TopK selection on all  $F$  components (modes) in the frequency domain. For the  $t$ -th time step, all the  $K$  significant ( $K < F$ ) components  $\hat{u}_K(t)$  are retained and form the truncated frequency domain. To be clarifying, we can present the forward procedure of  $k$ -th largest components  $\hat{u}_K(k, t)$  as:

$$\hat{u}_K(k, t) = \text{TopK}(\text{FFT}(\Psi[u(x^{(1)}, t), \dots, u(x^{(D)}, t)]^T)), \quad (1)$$

where  $\text{TopK}(\cdot)$  denotes the selection operator over  $F$  components,  $\Psi(\cdot)$  denotes the linear projection for the dimension alignment and the  $\text{FFT}(\cdot)$  operator is performed at the individual time step.

In the decoding stage, the predicted frequency domain features  $\hat{u}_K^{\text{pred}}(k, t)$  are adapted to the target shape using zero padding. Then, the inverse Fourier transform (IFFT) is applied to revert the frequency

domain features  $\hat{u}^{\text{pred}}(k, t)$  back to the spatial domain, ultimately obtaining the predicted physical field  $u^{\text{pred}}(x^{(d)}, t + 1)$  as:

$$u^{\text{pred}}(x^{(d)}, t + 1) = \Psi'(\text{IFFT}(\text{Zero-Padding}([\hat{u}_K^{\text{pred}}(1, t), \dots, \hat{u}_K^{\text{pred}}(K, t)]))). \quad (2)$$

This encoding and decoding process in the frequency domain is maintained throughout the whole OmniArch network. Since the encoding and decoding operations are always conducted along specific dimensions, thus we omit the  $d$ -th index indicator in the following context.

### 3.1.2 Transformer as an Integral Neural Operator

To achieve multi-physics versatility, we leverage the Transformer backbone to simulate integral neural operators. In physics, multi-physics systems often exhibit complex spatio-temporal dependencies, requiring effective long-range dependency modeling. The multi-head self-attention mechanism of the Transformer, with the introduction of the Temporal Mask, allows each time step to attend to all physical quantities at the same and previous time steps, enabling efficient temporal information integration. This design ensures the robustness and adaptability of the model in multi-physics systems. Additionally, by padding variable-length sequences, systems with different numbers of physical quantities can use the model for temporal regression predictions in batches, ensuring accuracy and stability.

Moreover, the autoregressive mechanism of the Transformer bears a strong mathematical resemblance to traditional multi-step methods for solving equations. Traditional multi-step methods approximate solutions iteratively, capturing the dynamic changes of the system. Similarly, the multi-head self-attention mechanism of the Transformer models the global dependencies at each time step, achieving precise capture of dynamic changes in the system.

Specifically, traditional multi-step methods for solving equations can be expressed iteratively as:

$$u^{\text{pred}}(x, t + 1) = u(x, t) + \Delta t \cdot f(u(x, t)). \quad (3)$$

In contrast, the autoregressive mechanism of the Transformer updates the current state by a weighted sum of previous time steps through attention weights:

$$u^{\text{pred}}(x, t + 1) = \sum_{i=1}^t \alpha_{i,t} \cdot u(x, i) = u(x, t) + \sum_{i=1}^{t-1} \alpha_{i,t-1} u(x, i), \quad (4)$$

where  $\alpha_{i,t}$  refer to the attention weights. Both approaches update based on previous time steps, with the attention mechanism acting as a neural surrogate [33] for the integral operator  $f$ .

Assume that we have a physical system with two physical quantities  $u(x, t)$  and  $v(x, t)$ , where the total number of quantities is recorded by  $C = 2$ . In OmniArch's computation, the frequency domain features  $\hat{u}_K(k, t)$  and  $\hat{v}_K(k, t)$  obtained from the Fourier Encoder are further transformed into real-valued embeddings through  $\mathcal{R}(\cdot)$ , resulting in the input embeddings for the Transformer  $\mathbf{U}_t$  and  $\mathbf{V}_t$ . These embeddings are grouped by time steps to form the input sequence  $\mathbf{Z}_t$ . For each time step  $t$ ,

$$\mathbf{Z}_t = \{\mathbf{U}_t, \mathbf{V}_t\} = \{\mathcal{R}(\hat{u}_K(k, t)), \mathcal{R}(\hat{v}_K(k, t))\}. \quad (5)$$

The Temporal Mask  $\mathbf{M}$  ensures that each time step  $t$  can access all physical quantities at the current and previous time steps, which is defined as:

$$\mathbf{M}(i, j) = \begin{cases} 0 & \text{if } \lfloor \frac{j}{C} \rfloor \leq \lfloor \frac{i}{C} \rfloor, \\ -\infty & \text{if } \lfloor \frac{j}{C} \rfloor > \lfloor \frac{i}{C} \rfloor, \end{cases} \quad (6)$$

where  $i$  and  $j$  represent the  $i$ -th and  $j$ -th tokens in the sequence, and  $\lfloor \frac{i}{C} \rfloor$  represents the time step. The input sequence then passes through multiple shared Transformer blocks, outputting the shifted right predicted feature sequence for each time step  $\{\hat{\mathbf{Z}}_t\}_{t=2}^{T+1}$ :

$$\{\hat{\mathbf{Z}}_t\}_{t=2}^{T+1} = \text{TransformerBlocks}(\{\mathbf{Z}_t\}_{t=1}^T, \mathbf{M}). \quad (7)$$

Due to numerical differences between dynamic systems, we use nRMSE to calculate the loss function  $L_{\text{sim}}$  for a batch during training:

$$L_{\text{sim}}^u = \frac{1}{|B|} \sqrt{\sum_{(x,t) \in B} \left( \frac{u^{\text{pred}}(x, t) - u(x, t)}{\sigma_u} \right)^2}, \quad L_{\text{sim}} = \frac{1}{C} \sum_{j \in C} L_{\text{sim}}^j. \quad (8)$$

This design can effectively capture the temporal evolution of physical fields, achieving high-precision dynamic system predictions and ensuring that systems with different numbers of physical quantities can adapt to this model for temporal regression predictions.

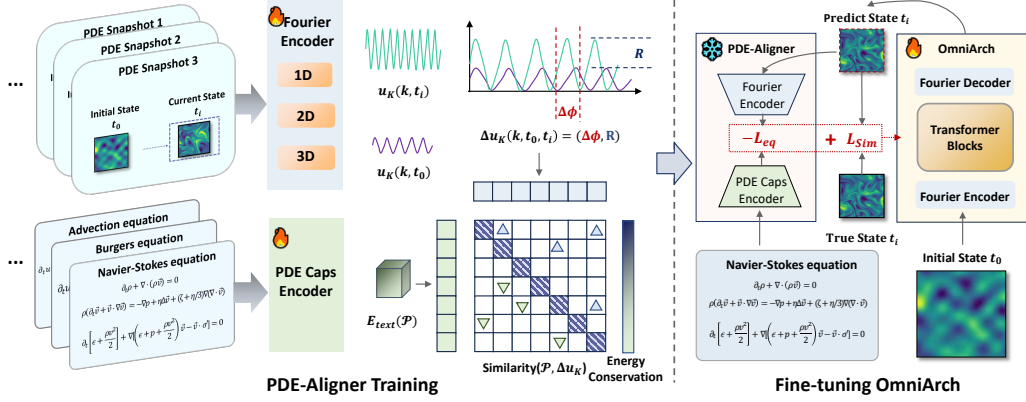


Figure 3: **(Left) PDE-Aligner** architecture with *Fourier Encoders* for initial/current state, and *PDE Caps Encoder* enforcing consistency via PDE constraints. **(Right) Fine-tuning OmniArch** with *PDE-Aligner* on downstream PDEs like Navier-Stokes equations for physics-informed learning.

### 3.2 Fine-tuning OmniArch: Enabling Physics-Informed Learning via Equation Supervision

The PDE equations are natural and intuitive ‘supervision’ methods for real-world physical phenomena. To perform the physical alignment, we incorporate the PDE-Aligner to achieve physics-informed learning. Unlike the pre-training stage, the OmniArch is designed to comply with specific physical laws during fine-tuning. As illustrated in Figure 3 (left), the PDE-Aligner employs a contrastive learning paradigm in the frequency domain. It compares the dynamic system’s semantics with statistical characters of the frequency domain, where the dynamical system descriptions, namely equations, boundaries, initial conditions, and other physical priors, are encoded into a representation  $E_{\text{text}}(\mathcal{P})$ . Then, we acquire the initial state  $u(x, t_0)$  and the current state  $u(x, t_i)$  of the physical field, applying the Fourier Encoder to obtain their  $k$ -th frequency domain representations  $\hat{u}_K(k, t_i)$  and  $\hat{u}_K(k, t_0)$ . We use the phase difference  $\Delta\phi = (\hat{u}_K(k, t_i) \cdot \hat{u}_K^*(k, t_0)) / (|\hat{u}_K(k, t_i)| |\hat{u}_K(k, t_0)|)$  and magnitude ratio  $R = |\hat{u}_K(k, t_i)| / |\hat{u}_K(k, t_0)|$ . Thus, we have the alignment loss function as:

$$L_{\text{Align}} = L_{\text{eq}} + \lambda L_E, \quad L_{\text{eq}} = \mathcal{S}(E_{\text{text}}(\mathcal{P}), \Psi[\Delta\phi, R]^\top), \quad L_E = \left| \sum_K R - 1 \right|. \quad (9)$$

where  $\lambda$  is a hyperparameter balancing the energy conservation loss. By minimizing the alignment loss function  $L_{\text{Align}}$ , the PDE-Aligner aligns the changes in the physical field with the textual descriptions within the constraints of energy conservation. In the fine-tuning stage (Figure 3 Right), the pre-trained PDE-Aligner can be used to measure the alignment between the predicted physical field and the textual description of the given physical system. Recalling the  $L_{\text{sim}}$  loss in Eq.(8), we reset the loss function for fine-tuning as  $L_{\text{ft}} = L_{\text{sim}} - L_{\text{eq}}$ .

## 4 Experiments

### 4.1 Dataset and Baselines

**Dataset.** We collect 1D, 2D, and 3D datasets from the public PDEBench and PDEArena. The 1D datasets include: (1) **CFD**, generated by the compressible Navier-Stokes equation with velocity ( $V_x$ ), density, and pressure. (2) **Bur.**, the Burgers’ equation with velocity. (3) **Diff.**, the diffusion-sorption equation with concentration ( $\rho$ ). (4) **Adv.**, the advection equation with velocity ( $V_x$ ). (5) **Reac.** the reaction-diffusion equation with concentration ( $\rho$ ). The 2D datasets include: (6) **CFD**, generated by the compressible Navier-Stokes equation with velocities ( $V_x, V_y$ ), density, and pressure. (7) **Reac.**, the reaction-diffusion equation with activator ( $u$ ) and inhibitor ( $v$ ). (8) **SWE**, the shallow-water equation with velocities ( $h$ ). (9) **Incom.**, generated by 2D Inhomogeneous, Incompressible Navier-Stokes equations, with velocities ( $V_x, V_y$ ) and particles. The 3D datasets include: (10) **CFD**, generated by the compressible Navier-Stokes equation with velocities ( $V_x, V_y, V_z$ ), density, and pressure. (11) **Maxw.**, the Maxwell equation with electric displacement ( $D_x, D_y, D_z$ ) and magnetic field ( $H_x, H_y, H_z$ ). More details can be found in Appendix C.

Table 1: The nRMSE on various PDEs. We evaluate base-size(-B) and large-size(-L). The previous state-of-the-art performance is underlined and our best performance is **bolded**.

Methods	1D					2D				3D	
	CFD	Adv.	Bur.	Diff.	Reac.	CFD	Reac.	SWE	Incom	CFD	Maxw.
<i>Baselines - Task specific Expert Models</i>											
<b>PINNs</b>	/	0.8130	0.9450	0.2200	0.2140	/	1.6000	0.0170	/	/	/
<b>U-Net</b>	2.6700	0.7760	0.3201	0.1507	0.0026	1.0700	0.8401	0.0830	1.1200	0.7989	0.2999
<b>FNO</b>	<u>1.4100</u>	<u>0.0091</u>	<u>0.0174</u>	<u>0.0017</u>	<u>0.0005</u>	0.2060	0.1203	0.0044	<u>0.2574</u>	<u>0.3052</u>	<u>0.1906</u>
<i>Baselines - Unified Pre-training and Fine-tuning</i>											
<b>PDEformer-1</b>	-	<u>0.0043</u>	<u>0.0095</u>	-	0.0009	-	-	-	-	-	-
<b>ORCA-SWIN-B</b>	-	-	-	-	-	/	0.8201	0.0062	/	-	-
<b>MPP-AVIT-B</b>	-	-	-	-	-	0.0227	0.0106	0.0024	/	-	-
<b>MPP-AVIT-L</b>	-	-	-	-	-	<u>0.0178</u>	<u>0.0098</u>	<u>0.0022</u>	/	-	-
<i>Full Pre-Training on 1D,2D,3D Data</i>											
<b>OmniArch-B(Ours)</b>	0.0340	0.0238	0.0089	0.0020	0.0006	0.0196	0.0158	0.0016	0.1726	0.5209	0.2834
<b>OmniArch-L(Ours)</b>	0.0250	0.0182	0.0063	0.0015	0.0004	0.0148	0.0105	0.0014	0.1494	0.4531	0.2268
<i>+ PDE-Aligner Fine-tuning</i>											
<b>OmniArch-B(Ours)</b>	0.0302	0.0201	0.0071	0.0017	0.0003	0.0153	0.0102	0.0015	0.0955	0.4032	0.1813
<b>OmniArch-L(Ours)</b>	<b>0.0200</b>	<b>0.0041</b>	<b>0.0032</b>	<b>0.0006</b>	<b>0.0002</b>	<b>0.0125</b>	<b>0.0084</b>	<b>0.0012</b>	<b>0.0827</b>	0.3723	<b>0.1671</b>
<b>std. <math>\pm</math></b>	0.0031	0.0012	0.0004	0.0001	0.0001	0.0017	0.0004	0.0003	0.0023	0.0443	0.0197
<b>Improvement <math>\uparrow</math></b>	<b>98.70%</b>	4.65%	66.32%	64.75%	60.00%	29.70%	14.28%	45.45%	67.87%	-	12.32%

Notes: Symbol ‘/’ means model did not converge while ‘-’ means model not applicable to this dataset.

**Baselines.** The baselines are divided into two categories: (1) *Task-specific expert models*, which include Physics-Informed Neural Networks (PINNs) [26], U-Net [29], and Fourier Neural Operator (FNO) [12], all of which require training from scratch for each specific case (each equation/coefficient, etc.). (2) *Unified pre-training models*, which include PDEformer-1 [39], Multiple Physics Pre-training (MPP) [17] and a SWIN-transformer [13] used for the ORCA task. More details on the baselines are provided in Appendix D.

**Training Details.** The OmniArch model uses single-layer encoders and decoders for data of various dimensions, with the LLaMA model (trained from scratch) as the shared Transformer architecture. The PDE-Aligner employs the pre-trained Fourier encoder from OmniArch to encode physical fields and the pre-trained BERT-base-based model to encode PDE captions. Two versions of the model are provided: Base and Large. Additional training details are available in Appendix E.

## 4.2 Results and Analysis

OmniArch is designed to support multi-scale, multi-physics, and flexible physics alignment. Table 1 presents the normalized root mean square error (nRMSE) across various PDEs for different methods.

**Multi-Physics Results.** (1) Compared with Task-specific Expert Models. PINNs, U-Net, and FNO require training from scratch for each specific equation or coefficient. While FNO shows strong performance, PINNs and U-Net struggle with convergence and accuracy in some cases (Like the CFD-1D, and CFD-2D). (2) Compared with Unified Pre-training Models. PDEformer-1 exhibits proficiency in specific 1D equations but fails to generalize beyond its formulation structure. MPP and ORCA-SWIN leverage 2D pre-training and fine-tuning, improving generalization, yet their effectiveness remains constrained by the diversity of the pre-training data. (3) OmniArch Performance. OmniArch, pre-trained on 1D, 2D, and 3D data, demonstrates superior performance across all evaluated datasets. Both the base (B) and large (L) versions of OmniArch outperform existing models, validating its

Table 2: The Performance on Zero-shot PDEs.

Methods	Shock	KH	OTVortex
FNO	0.7484	1.0891	0.5946
U-Net	1.6667	0.1677	0.4217
MPP-L	0.3243	1.3261	0.3025
<b>OmniArch-L</b>	<b>0.2126</b>	<b>0.2763</b>	<b>0.1718</b>

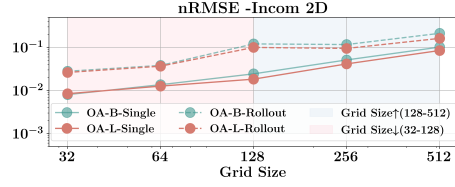


Figure 4: The multi-scale capability.

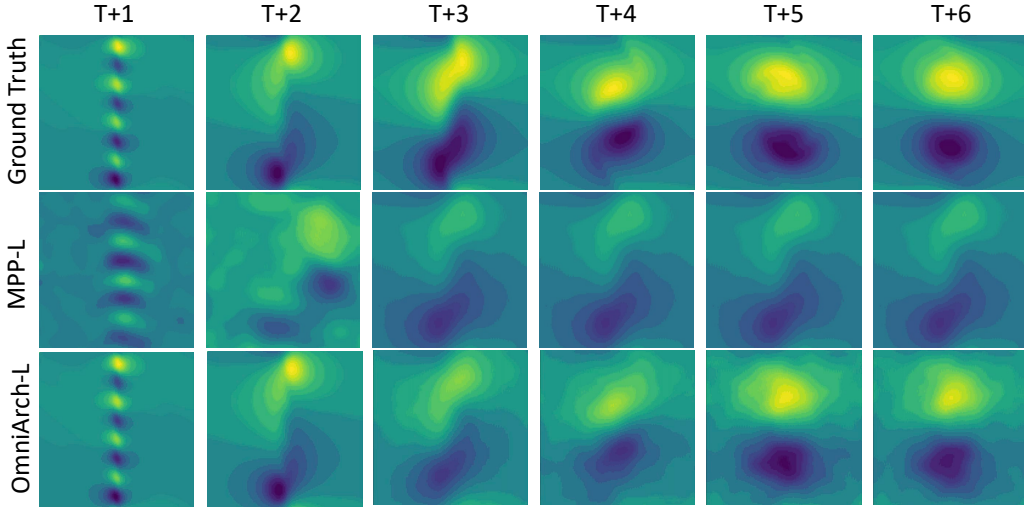


Figure 5: Zero-shot prediction results (Rollout) of OmniArch-L and MPP-L on KH dataset. Displaying time steps T+1 to T+6, the top row shows ground truth data, while the middle and the bottom row illustrate MPP-L’s and OmniArch-L’s predictions respectively.

robustness in multi-physics contexts. (4) PDE-Aligner Fine-tuning. Fine-tuning with PDE-Aligner significantly enhances OmniArch’s accuracy, particularly for complex datasets. This step utilizes a pre-trained Fourier encoder and BERT-base-based model, ensuring precise alignment between physical fields and PDE descriptions. OmniArch demonstrates substantial performance gains over baselines, with up to 98.70% improvement on CFD-1D and notable enhancements across other PDEs. These results corroborate its superior multi-physics generalization driven by comprehensive pre-training and effective physics-language alignment through PDE-Aligner.

**Multi-scale Results.** In Figure 4, we present the multi-scale inference performance of OmniArch-Base and OmniArch-Large on the 2D Incom. Dataset. Due to the frequency truncation capability of the Fourier Encoder, OmniArch can handle inputs of varying grid sizes without requiring re-training. In the red-shaded area, the nRMSE decreases as the grid size becomes smaller. Conversely, in the blue-shaded area, the nRMSE slightly increases. However, even with a grid size of 512, the maximum nRMSE remains below 0.2. In the rollout settings, a grid size of 256 sometimes leads to better or comparable performance to a grid size of 128. Additional visualizations are provided in Appendix H.5.

**Flexible Physics Alignment.** To verify the PDE-Aligner’s ability to perceive physical information, we equipped it with a classification head to classify physical fields. In Figure 6, the PDE-Aligner can perceive physical field categories based on equation text information and physical field features, and the classification accuracy rate exceeds 0.94 on all ten categories. More details are in Appendix F.3.

**Zero-shot Performance.** Our examination of 2D PDE predictions, as illustrated in Figure 5, reveals that OmniArch effectively captures both low- and high-frequency patterns even in zero-shot scenarios, surpassing former 2D models like MPP. MPP often misses key features, leading to erroneous representations of the primary physics and failed rollouts. Details on the zero-shot dataset, including shock wave, KH, and OTVortex phenomena, are provided in Appendix C.2.

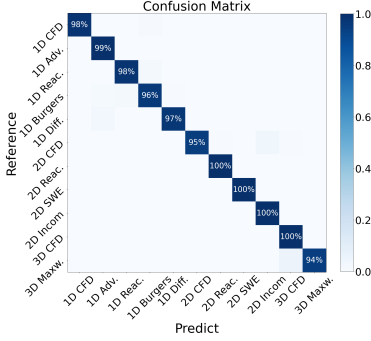


Figure 6: PDE-Aligner Acc.

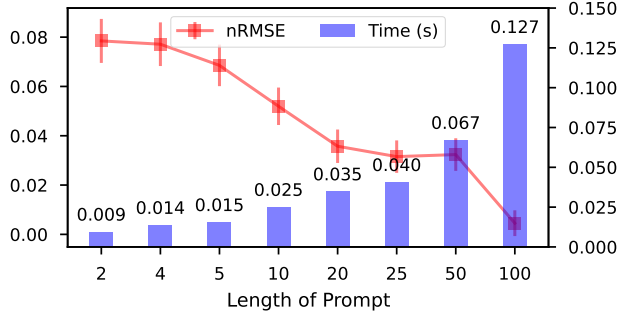


Figure 7: In-context learning on SWE with OmniArch-B.

As shown in Table 2, nRMSE scores indicate that all models, except OmniArch, tend to underperform in zero-shot transfer. This suggests that OmniArch’s use of Fourier Encoders and unified training approach enhances its ability to generalize across different PDEs. By leveraging flexible grid inputs and dynamic observation windows during pre-training, OmniArch effectively captures the underlying physics of the observed field states, which may not be adequately addressed by methods adhering strictly to explicit grid and temporal dependencies.

**In-Context Learning.** After auto-regressively pre-trained on various dynamic systems, we observe that OmniArch could learn neural operators within the observations of several time steps, which is similar to the in-context learning in Large Language Models. Here, we define the given time-series of observations as *PDE Prompt*. Our approach varies the prompt length from 2 tokens (derived from a 50 time step interval) to 100 tokens (from a 1 time step interval). As indicated in Figure 7, longer prompts yield higher precision with less variance, while shorter prompts can expedite inference by up to 10 times compared to full-length prompts. More details are in Appendix H.2.

**Fine-tuning for Inverse Problems.** Demonstrating a model’s capability to infer hidden physical parameters from known equations is a critical test of its ability to learn underlying physics. The results in Table 3 demonstrate that OmniArch outperforms MPP in parameter estimation tasks, with lower RMSE values indicating more accurate predictions. Models trained from scratch yield the highest errors, underscoring the effectiveness of our fine-tuning approach. This evidence supports the notion that OmniArch is not only proficient in forward simulations but also exhibits superior performance in deducing hidden dynamics within complex systems. More details are in Appendix H.3.

**Other Results.** In addition to the primary experiments, we include more rollout case studies in Appendix H.4 and report the inference-time GPU Memory usage compared with baselines in Appendix H.7. We also include ablation studies for training settings in Appendix G and the detailed performance for CFD PDEs in Appendix H.6. These additional evaluations highlight OmniArch’s robustness and accuracy in complex physical simulations, surpassing other state-of-the-art models.

## 5 Conclusion

In this study, we introduced a pioneering foundation model for scientific computing, specifically tailored for the resolution of partial differential equations (PDEs). By integrating this model with a novel PDE-Aligner for fine-tuning, we have established new state-of-the-art benchmarks across a comprehensive suite of tasks within the PDEBench. Additionally, we investigated the zero-shot learning capabilities of our pre-trained model, uncovering a degree of transferability that mirrors the emergent properties found in large-scale language models. Despite the successes, we recognize the challenges posed by 3D PDE systems to our OmniArch model, which may leave for future research. We envisage that OmniArch will serve as a cornerstone for developing foundation models in the domain of PDE learning, fostering a significant convergence between scientific machine learning (SciML) and broader deep learning disciplines.

Table 3: nRMSE for Inverse Problems.

Methods	Forcing	Buoyancy
<b>MPP</b>	$0.2 \pm 0.008$	$0.78 \pm 0.006$
<b>OmniArch</b>	$0.16 \pm 0.005$	$0.73 \pm 0.012$
<b>Scratch</b>	$0.39 \pm 0.012$	$0.83 \pm 0.027$

## References

- [1] Kelsey R. Allen, Tatiana Lopez-Guevara, Kimberly L. Stachenfeld, Alvaro Sanchez-Gonzalez, Peter W. Battaglia, Jessica B. Hamrick, and Tobias Pfaff. Physical design using differentiable learned simulators. CoRR, abs/2202.00728, 2022.
- [2] E Oran Brigham. The fast Fourier transform and its applications. Prentice-Hall, Inc., 1988.
- [3] Tom Brown, Benjamin Mann, Nick Ryder, Melanie Subbiah, Jared D Kaplan, Prafulla Dhariwal, Arvind Neelakantan, Pranav Shyam, Girish Sastry, Amanda Askell, et al. Language models are few-shot learners. Advances in neural information processing systems, 33:1877–1901, 2020.
- [4] Ting Chen, Simon Kornblith, Mohammad Norouzi, and Geoffrey Hinton. A simple framework for contrastive learning of visual representations. In International conference on machine learning, pages 1597–1607. PMLR, 2020.
- [5] Salvatore Cuomo, Vincenzo Schiano Di Cola, Fabio Giampaolo, Gianluigi Rozza, Maziar Raissi, and Francesco Piccialli. Scientific machine learning through physics-informed neural networks: Where we are and what’s next. Journal of Scientific Computing, 92(3):88, 2022.
- [6] Jacob Devlin, Ming-Wei Chang, Kenton Lee, and Kristina Toutanova. Bert: Pre-training of deep bidirectional transformers for language understanding. arXiv preprint arXiv:1810.04805, 2018.
- [7] Getao Du, Xu Cao, Jimin Liang, Xueli Chen, and Yonghua Zhan. Medical image segmentation based on u-net: A review. Journal of Imaging Science and Technology, 2020.
- [8] Jayesh K. Gupta and Johannes Brandstetter. Towards multi-spatiotemporal-scale generalized PDE modeling. CoRR, abs/2209.15616, 2022.
- [9] George Em Karniadakis, Ioannis G Kevrekidis, Lu Lu, Paris Perdikaris, Sifan Wang, and Liu Yang. Physics-informed machine learning. Nature Reviews Physics, 3(6):422–440, 2021.
- [10] Yinheng Li. A practical survey on zero-shot prompt design for in-context learning. In Ruslan Mitkov and Galia Angelova, editors, Proceedings of the 14th International Conference on Recent Advances in Natural Language Processing, RANLP 2023, Varna, Bulgaria, 4-6 September 2023, pages 641–647. INCOMA Ltd., Shoumen, Bulgaria, 2023.
- [11] Zijie Li, Dule Shu, and Amir Barati Farimani. Scalable transformer for PDE surrogate modeling. CoRR, abs/2305.17560, 2023.
- [12] Zongyi Li, Nikola Kovachki, Kamyar Azizzadenesheli, Burigede Liu, Kaushik Bhattacharya, Andrew Stuart, and Anima Anandkumar. Fourier neural operator for parametric partial differential equations. arXiv preprint arXiv:2010.08895, 2020.
- [13] Ze Liu, Yutong Lin, Yue Cao, Han Hu, Yixuan Wei, Zheng Zhang, Stephen Lin, and Baining Guo. Swin transformer: Hierarchical vision transformer using shifted windows. In 2021 IEEE/CVF International Conference on Computer Vision, ICCV 2021, Montreal, QC, Canada, October 10-17, 2021, pages 9992–10002. IEEE, 2021.
- [14] Cooper Lorsung, Zijie Li, and Amir Barati Farimani. Physics informed token transformer. CoRR, abs/2305.08757, 2023.
- [15] Lu Lu, Pengzhan Jin, Guofei Pang, Zhongqiang Zhang, and George Em Karniadakis. Learning nonlinear operators via deepnet based on the universal approximation theorem of operators. Nature machine intelligence, 3(3):218–229, 2021.
- [16] Lu Lu, Xuhui Meng, Zhiping Mao, and George Em Karniadakis. Deepxde: A deep learning library for solving differential equations. SIAM review, 63(1):208–228, 2021.
- [17] Michael McCabe, Bruno Régaldo-Saint Blancard, Liam Holden Parker, Ruben Ohana, Miles D. Cranmer, Alberto Bietti, Michael Eickenberg, Siavash Golkar, Géraud Krawezik, François Lanusse, Mariel Pettee, Tiberiu Tesileanu, Kyunghyun Cho, and Shirley Ho. Multiple physics pretraining for physical surrogate models. CoRR, abs/2310.02994, 2023.
- [18] Grégoire Mialon, Quentin Garrido, Hannah Lawrence, Danyal Rehman, Yann LeCun, and Bobak Toussi Kiani. Self-supervised learning with lie symmetries for partial differential equations. CoRR, abs/2307.05432, 2023.

- [19] Eric Nguyen, Michael Poli, Marjan Faizi, Armin W. Thomas, Michael Wornow, Callum Birch-Sykes, Stefano Massaroli, Aman Patel, Clayton M. Rabideau, Yoshua Bengio, Stefano Ermon, Christopher Ré, and Stephen Baccus. Hyenadna: Long-range genomic sequence modeling at single nucleotide resolution. In Alice Oh, Tristan Naumann, Amir Globerson, Kate Saenko, Moritz Hardt, and Sergey Levine, editors, Advances in Neural Information Processing Systems 36: Annual Conference on Neural Information Processing Systems 2023, NeurIPS 2023, New Orleans, LA, USA, December 10 - 16, 2023, 2023.
- [20] J. Tinsley Oden. An introduction to the finite element method with applications to nonlinear problems (R. e. white). SIAM Rev., 31(3):512, 1989.
- [21] Jaideep Pathak, Shashank Subramanian, Peter Harrington, Sanjeev Raja, Ashesh Chattopadhyay, Morteza Mardani, Thorsten Kurth, David Hall, Zongyi Li, Kamyar Azizzadenesheli, Pedram Hassanzadeh, Karthik Kashinath, and Animashree Anandkumar. Fourcastnet: A global data-driven high-resolution weather model using adaptive fourier neural operators. CoRR, abs/2202.11214, 2022.
- [22] Tobias Pfaff, Meire Fortunato, Alvaro Sanchez-Gonzalez, and Peter W Battaglia. Learning mesh-based simulation with graph networks. arXiv preprint arXiv:2010.03409, 2020.
- [23] Alec Radford, Jong Wook Kim, Chris Hallacy, Aditya Ramesh, Gabriel Goh, Sandhini Agarwal, Girish Sastry, Amanda Askell, Pamela Mishkin, Jack Clark, Gretchen Krueger, and Ilya Sutskever. Learning transferable visual models from natural language supervision. In Marina Meila and Tong Zhang, editors, Proceedings of the 38th International Conference on Machine Learning, ICML 2021, 18-24 July 2021, Virtual Event, volume 139 of Proceedings of Machine Learning Research, pages 8748–8763. PMLR, 2021.
- [24] Alec Radford, Karthik Narasimhan, Tim Salimans, Ilya Sutskever, et al. Improving language understanding by generative pre-training. OpenAI blog, 2018.
- [25] Alec Radford, Jeffrey Wu, Rewon Child, David Luan, Dario Amodei, Ilya Sutskever, et al. Language models are unsupervised multitask learners. OpenAI blog, 1(8):9, 2019.
- [26] Maziar Raissi, Paris Perdikaris, and George E. Karniadakis. Physics-informed neural networks: A deep learning framework for solving forward and inverse problems involving nonlinear partial differential equations. J. Comput. Phys., 378:686–707, 2019.
- [27] Bogdan Raonic, Roberto Molinaro, Tim De Ryck, Tobias Rohner, Francesca Bartolucci, Rima Alaifari, Siddhartha Mishra, and Emmanuel de Bézenac. Convolutional neural operators for robust and accurate learning of pdes. In Alice Oh, Tristan Naumann, Amir Globerson, Kate Saenko, Moritz Hardt, and Sergey Levine, editors, Advances in Neural Information Processing Systems 36: Annual Conference on Neural Information Processing Systems 2023, NeurIPS 2023, New Orleans, LA, USA, December 10 - 16, 2023, 2023.
- [28] Anja Reusch, Maik Thiele, and Wolfgang Lehner. Transformer-encoder and decoder models for questions on math. In Guglielmo Faggioli, Nicola Ferro, Allan Hanbury, and Martin Potthast, editors, Proceedings of the Working Notes of CLEF 2022 - Conference and Labs of the Evaluation Forum, Bologna, Italy, September 5th - to - 8th, 2022, volume 3180 of CEUR Workshop Proceedings, pages 119–137. CEUR-WS.org, 2022.
- [29] Olaf Ronneberger, Philipp Fischer, and Thomas Brox. U-net: Convolutional networks for biomedical image segmentation. In Medical Image Computing and Computer-Assisted Intervention–MICCAI 2015: 18th International Conference, Munich, Germany, October 5-9, 2015, Proceedings, Part III 18, pages 234–241. Springer, 2015.
- [30] Junhong Shen, Liam Li, Lucio M Dery, Corey Staten, Mikhail Khodak, Graham Neubig, and Ameet Talwalkar. Cross-modal fine-tuning: Align then refine. In International Conference on Machine Learning, pages 31030–31056. PMLR, 2023.
- [31] Nahian Siddique, Sidike Paheding, Colin P Elkin, and Vijay Devabhaktuni. U-net and its variants for medical image segmentation: A review of theory and applications. Ieee Access, 9:82031–82057, 2021.
- [32] Shashank Subramanian, Peter Harrington, Kurt Keutzer, Wahid Bhimji, Dmitriy Morozov, Michael W. Mahoney, and Amir Gholami. Towards foundation models for scientific machine learning: Characterizing scaling and transfer behavior. CoRR, abs/2306.00258, 2023.

- [33] Luning Sun, Han Gao, Shaowu Pan, and Jian-Xun Wang. Surrogate modeling for fluid flows based on physics-constrained deep learning without simulation data. Computer Methods in Applied Mechanics and Engineering, 361:112732, 2020.
- [34] Makoto Takamoto, Timothy Praditia, Raphael Leiteritz, Daniel MacKinlay, Francesco Alesiani, Dirk Pflüger, and Mathias Niepert. Pdebench: An extensive benchmark for scientific machine learning. In Sanmi Koyejo, S. Mohamed, A. Agarwal, Danielle Belgrave, K. Cho, and A. Oh, editors, Advances in Neural Information Processing Systems 35: Annual Conference on Neural Information Processing Systems 2022, NeurIPS 2022, New Orleans, LA, USA, November 28 - December 9, 2022, 2022.
- [35] Hugo Touvron, Thibaut Lavril, Gautier Izacard, Xavier Martinet, Marie-Anne Lachaux, Timothée Lacroix, Baptiste Rozière, Naman Goyal, Eric Hambro, Faisal Azhar, Aurélien Rodriguez, Armand Joulin, Edouard Grave, and Guillaume Lample. Llama: Open and efficient foundation language models. CoRR, abs/2302.13971, 2023.
- [36] Petar Veličković, Guillem Cucurull, Arantxa Casanova, Adriana Romero, Pietro Lio, and Yoshua Bengio. Graph attention networks. arXiv preprint arXiv:1710.10903, 2017.
- [37] Liu Yang, Siting Liu, Tingwei Meng, and Stanley J Osher. In-context operator learning with data prompts for differential equation problems. Proceedings of the National Academy of Sciences, 120(39):e2310142120, 2023.
- [38] Liu Yang, Tingwei Meng, Siting Liu, and Stanley J. Osher. Prompting in-context operator learning with sensor data, equations, and natural language. CoRR, abs/2308.05061, 2023.
- [39] Zhanhong Ye, Xiang Huang, Leheng Chen, Hongsheng Liu, Zidong Wang, and Bin Dong. Pdeformer: Towards a foundation model for one-dimensional partial differential equations. CoRR, abs/2402.12652, 2024.
- [40] Duo Zhang, Hangrui Bi, Fu-Zhi Dai, Wanrun Jiang, Linfeng Zhang, and Han Wang. DPA-1: pretraining of attention-based deep potential model for molecular simulation. CoRR, abs/2208.08236, 2022.
- [41] Shengyu Zhang, Linfeng Dong, Xiaoya Li, Sen Zhang, Xiaofei Sun, Shuhe Wang, Jiwei Li, Runyi Hu, Tianwei Zhang, Fei Wu, and Guoyin Wang. Instruction tuning for large language models: A survey. CoRR, abs/2308.10792, 2023.

## Appendix

### A Table of notations

A table of notations is given in Table 4.

Table 4: Table of notations

<b>Basic Notations</b>	
$x, t$	Spatial and Temporal coordinate (time)
$\Delta t$	Time interval
$T$	Total time steps
$D$	Total dimensions of physical fields
$C$	Number of physical fields
$B$	Batch size
$\mathcal{U}$	Physical field inputs
$u(x^{(d)}, t)$	Physical field of dimension $d$ at spatial coordinate $x$ and time $t$
$\Psi(\cdot)$	Linear projection
<b>OmniArch Related Notations</b>	
$\mathcal{F}, \mathcal{F}^{-1}$	Fourier transformation and its inverse
$F$	Components (modes) in the frequency domain
$\hat{\mathcal{U}}$	Physical field frequency domain representation
$k$	Frequency Variable
$K$	Number of retained Fourier modes (cut-off frequency)
$\hat{u}(k, t)$	Fourier transform of $u(x, t)$ at frequency $k$ and time $t$
$\hat{u}_K(k, t)$	Truncated Fourier modes (TopK modes) at frequency $k$ and time $t$
$\hat{u}_K^{\text{pred}}(k, t)$	Predicted Fourier modes at frequency $k$ and time $t$
$u^{\text{pred}}(x, t)$	Predicted physical field at spatial coordinate $x$ and time $t$
$f(\cdot)$	Integral operator
$\alpha_{i,t}$	Attention weights at spatial coordinate $i$ and time $t$
$\mathcal{R}(\cdot)$	Real-valued embedding function of the frequency domain features
$U_t, V_t$	Physical field embedding token from $\mathcal{R}$ at time $t$
$\mathbf{Z}_t$	Input sequence consist of grouped embeddings from $U_t, V_t$
$\hat{\mathbf{Z}}_t$	Shifted right predicted feature sequence
$\mathbf{M}$	Temporal mask used in Transformer Blocks
$\sigma_u$	Variance of physical field $u$
$L_{\text{sim}}^u$	nRMSE loss of physical field $u$
$L_{\text{sim}}$	nRMSE loss of all physical fields
<b>PDE-Aligner Related Notations</b>	
$\mathcal{P}$	PDE text description (captions)
$E_{\text{text}}(\cdot)$	Text encoder used for PDE captions
$\Delta\phi$	Phase difference between the initial state and current state
$R$	Amplitude ratio between two states
$\lambda$	The hyperparameter balancing the the energy conservation loss
$L_{\text{eq}}$	Similarity between text embedding and physical embedding
$L_{\text{E}}$	Energy conservation loss
$L_{\text{Align}}$	PDE-Aligner training loss
$L_{\text{ft}}$	OmniArch fine-tune loss

### B Limitations

Despite its advancements, OmniArch remains fundamentally data-driven, and its interpretability requires further improvement, even with the PDE-Aligner enhancing physical prior alignment. Constraints in computational power and data availability have limited OmniArch’s scalability, affecting

its generalization capabilities, particularly in complex and abrupt dynamical systems such as 3D tasks and shock wave PDEs. Addressing these limitations is crucial for further development and broader applicability in scientific and engineering contexts.

## C Dataset details

### C.1 OmniArch Pre-training Dataset

**Pre-training Stage.** We structured the PDEBench data into distinct training, validation, and testing subsets. For one-dimensional (1D) PDEs, the training dataset comprises a selection from the CFD-1D, ReacDiff, Advection, Burgers, and diff-sorp datasets. From these, we reserve a random 10% sample of trajectories as the in-domain test set for each respective PDE equation. The Shock Tube Equation is designated as the out-of-domain test set. Additionally, the test portions of the reacdiff and diff-sorp datasets are utilized as part of the test set.

In the two-dimensional (2D) PDE case, we allocate 90% of trajectories from the CFD, diff-react, NSincom, and shallow water datasets for training. The remaining 10% form the in-domain test set. The Shock Tube, Kelvin-Helmholtz instability (KH), and Tolman-Oppenheimer-Volkoff (TOV) scenarios are included as out-of-domain test sets.

For three-dimensional (3D) PDEs, 90% of trajectories from the CFD-3D dataset are utilized for training, with the remaining 10% serving as the in-domain test set. The complete datasets for blastwave and turbulence simulations are used as out-of-domain test sets. The Details of our pre-training dataset can be found in Table 5.

Table 5: Data Statistics for OmniArch Pre-training

Dataset	#Train	#Validation	#Physical quantities	$N_t$	$N_s$	
1D	CFD	45000	5000	velocities $V_x$ , density, pressure	100	1024
	Reac.	144000	16000	concentration $\rho$	200	1024
	Adv.	72000	8000	velocities $V_x$	200	1024
	Bur.	108000	12000	velocities $V_x$	200	1024
	Diff.	9000	1000	concentration $\rho$	100	1024
2D	CFD	39600	4400	velocities $V_x, V_y$ , density, pressure	21	512
	Reac.	900	100	activator $u$ , inhibitor $v$	100	128
	Incom	900	100	velocities $V_x, V_y$ , particle	1000	256
	SWE	900	100	velocities $h$	100	128
3D	CFD	630	70	velocities $V_x, V_y, V_z$ , density, pressure	21	128
	Maxw.	8640	960	electric displacement $D_x, D_y, D_z$ magnetic field $H_x, H_y, H_z$	8	64

### C.2 Dataset For Zero-shot Learning

We choose three test datasets from PDEBench to validate the zero-shot ability of our model. They all belong to two-dimensional compressible Navier-Stokes equations but are different fluid phenomena that exhibit distinct physical mechanisms and characteristics. Brief introductions and details of the datasets are as follows:

- **OTVortex:** The Orszag-Tang Vortex system is a compressible flow problem that generates highly complex vortex structures through the careful selection of initial conditions. The dataset includes one example, which is a  $1024 \times 1024$  resolution physical field evolved over 101 time steps with a time interval of 0.01.
- **2D Shock:** Shock waves are characterized by abrupt changes in flow properties resulting from sudden discontinuities in fluid flow, such as rapid changes in pressure, temperature, and density. The dataset includes one example, which is also a  $1024 \times 1024$  resolution physical field evolved over 101 time steps with a time interval of 0.01.

- **2D KH:** The Kelvin-Helmholtz instability is a fluid instability that occurs at the interface between two fluid layers with different velocities or densities. This dataset consists of seven examples generated based on different parameters  $M$ ,  $dk$ , and  $Re$ . Each is a  $1024 \times 1024$  resolution physical field evolved over 51 time steps with a time interval of 0.1. We conducted experiments on all samples and averaged the results.

## D Baseline implementation details

In our experiments, we adopt the benchmarking framework provided by PDEBench [34] and select three well-established methods for comparative analysis. Furthermore, we have incorporated the Multiple Physics Pre-training (MPP) model into our comparative analysis to address the need for retraining that is inherent to the aforementioned methods when faced with novel sets of conditions, the detailed training hyperparameters of FNO, U-Net, and PINN is provided in Table 6, following PDEbench [34]. The first hyperparameter of U-Net is the unroll steps (denoted as **us**), and the second is the train steps (denoted as **ts**). The hyperparameters shared by both FNO and U-Net are the initial steps (denoted as **is**) and batch size (denoted as **bs**). The hyperparameter in PINNs is the hidden size (denoted as **hid**). The learning rate, shared by FNO, U-Net, and PINNs, is denoted as **lr**.

Table 6: Setting details when training FNO, U-Net, and PINN, \* means shared setting for FNO and U-Net, shared setting for FNO, U-Net, and PINN is denoted with a symbol †.

		FNO		U-Net		is*	bs*	PINNs	lr†
		modes	width	us	ts			hid	
<b>1D</b>	<b>Adv.</b>	12	20	20	200	10	50	40	0.001
	<b>Bur.</b>	12	20	20	200	10	50	40	0.001
	<b>CFD</b>	12	20	20	100	10	50	40	0.001
	<b>Diff.</b>	12	20	20	101	10	50	40	0.001
	<b>Reac.</b>	12	20	20	101	10	50	40	0.001
<b>2D</b>	<b>CFD</b>	12	20	20	21	10	20	40	0.001
	<b>Reac.</b>	12	20	20	101	10	5	40	0.001
	<b>SWE</b>	12	20	20	101	10	5	40	0.001
	<b>Incom</b>	12	20	20	101	10	20	40	0.001
<b>3D</b>	<b>CFD</b>	12	20	20	21	10	5	40	0.001
	<b>Maxw.</b>	12	20	7	8	7	5	40	0.001

**Physics-Informed Neural Networks (PINNs)** [26]. PINNs utilize neural networks to solve differential equations by embedding physical laws into a multi-objective optimization framework, minimizing PDE residuals and boundary/initial condition errors [5].

**U-Net** [29]. U-Net, designed for biomedical image segmentation, uses an encoder-decoder structure for context capture and precise localization [31, 7]. We adapt U-Net into 1D and 3D forms to analyze spatio-temporal patterns in physical fields.

**Fourier Neural Operator (FNO)** [12]. FNO pioneers in learning function-to-solution mappings by parameterizing integral kernels in the Fourier domain, enabling efficient and accurate resolution-invariant neural operators.

**PDEformer-1** [39]. PDEformer-1 is a neural solver capable of simultaneously addressing various types of 1D partial differential equations. It uses a graph Transformer and implicit neural representation (INR) to generate mesh-free predicted solutions.

**Multiple Physics Pre-training (MPP)** [17]. MPP extends PDEBench’s 2D physics scenarios to learn versatile features for predicting dynamics across various physical systems and comprises pre-training and fine-tuning phases, warranting its inclusion in our comparative analysis.

**ORCA-SWIN** [30, 13]. ORCA fine-tunes the SWIN Transformer for different PDEs by first aligning the embedded feature distribution of the target PDE data with the pre-training modality, and then refining the model on this aligned data to effectively leverage shared knowledge across various PDEs.

## E OmniArch implementation details

### E.1 Pre-training OmniArch

In our training process, the following strategies or decisions were made:

- **Pre/Post Norm:** Pre-norm
- **Norm Type:** RMS Norm Type
- **Architecture:** Decoder-Only
- **Attention-Type:** Multi-scaled Attention
- **Position Embedding:** RoPE
- **Casual Masking:** True- We only evaluate the loss on the T + 1 physical files prediction.
- **Hidden Size:** 1024
- **initializer\_range:** 0.02
- **intermediate\_size:** 4096
- **num\_attention\_heads:** 16

Table 7: Detailed setting of hyperparameters in pre-training the base and large models. The batch sizes, modes, and widths are provided as lists, with values corresponding to 1D, 2D, and 3D data respectively.

Hyperparameters	Base	Large
#Layers	12	24
Hidden Size	768	1024
#Heads	12	16
Intermediate Size	3072	4096
#Params	316.13M	672.85M
Batch Sizes	[42,3,1]	[32,2,1]
Modes	[12,12,12]	[12,12,12]
Widths	[8,8,8]	[8,8,8]
Learning Rate	0.0001	0.0001
Scheduling Method	Cosine Annealing	Cosine Annealing

We trained two different sizes of model: base and large, which primarily differ in the number of layers, hidden sizes, number of heads, and intermediate sizes, as detailed in Figure 7. For the base model, we selected batch sizes of [42, 3, 1] for the 1D, 2D, and 3D trajectories, respectively. These batch sizes represent the maximum capacities our acceleration devices could handle while maintaining the ratio of data trajectories. This configuration allows for optimal training efficiency by minimizing idle time and maximizing device utilization. For the large model, due to its significantly increased size, we adjusted the batch sizes to [32, 2, 1] to ensure that the GPU memory is fully utilized. This reduction in batch sizes accommodates the larger model’s memory requirements while still enabling effective training across the different dimensions of data trajectories.

### E.2 Fine-tuning OmniArch

Fine-tuning is performed on an A40 GPU cluster, which has 40GiB of memory per device. The fine-tuning settings for each dataset are shown in Table 8. We set the learning rate to 1e-5, which results in fast convergence. Using 2 GPUs in Distributed Data-Parallel mode, we fine-tune each dataset for a maximum of 30 epochs and apply early stopping.

Table 8: Detailed Fine-tuning Settings: The table provides the learning rate, width, modes, and batch size for 1D, 2D, and 3D data.

Dims	learning rate	width	modes	batch size	Scheduling Method
1D	1e-5	8	12	64	Cosine Annealing
2D	1e-5	8	12	8	Cosine Annealing
3D	1e-5	8	12	2	Cosine Annealing

## F PDE-Aligner implementation details

### F.1 PDE-Aligner Pre-training Dataset

**PDE-Aligner equation augmentation.** Given the significant imbalance between equation caption data and physical field data, a single equation can yield a multitude of physical field simulations. To augment equation captions effectively, it is crucial to preserve the equation’s solutions and boundaries while adhering to physical laws and exploring a wide array of possible substitutions. To achieve this, we have developed a five-step augmentation pipeline: *Equation Rewriting*, *Form Transformation*, *Linear Combination*, *Symbol Substitution*, and *Physical Checking*:

- **Equation Rewriting.** We apply mathematical identities to modify the equation, ensuring the core properties remain intact.
- **Form Transformation.** We transform equations between differential and integral forms and employ techniques such as Green’s functions to broaden the equation’s representations.
- **Linear Combination.** For systems of equations, we derive new variants through linear combinations, enriching the dataset without altering the system’s nature.
- **Symbol Substitution.** We systematically swap variables with alternative symbols, such as replacing  $x$  with  $\xi$ , to maintain consistency and avoid ambiguity.
- **Physical Checking.** A panel of GPT-4-based experts evaluates the augmented equations, filtering out those that do not align with physical principles.

Leveraging the first four steps, we generate 200 augmented instances per equation type. Subsequently, during the Physical Checking phase, we select the top 50% of these examples based on quality for pre-training. Representative samples of the augmented examples are available in Appendix F.2.

Additionally, we randomly sample the numerical distributions of different physical quantities at two distinct time steps within the physical field to represent the field’s temporal variations. Each set of two-step physical field data is paired with a corresponding enhanced equation text to form a single data instance. This approach is used to compile a comprehensive pre-training dataset for the PDE-Aligner.

### F.2 Examples of Generated PDES

#### F.2.1 Burgers 1D

- Original form:

$$\begin{aligned} \partial_t u(t, x) + \partial_x (u^2(t, x)/2) &= \nu/\pi \partial_{xx} u(t, x), \quad x \in (0, 1), t \in (0, 2], \\ u(0, x) &= u_0(x), \quad x \in (0, 1), \end{aligned}$$

- After augmented:

$$0.77 \int \left( \frac{\partial}{\partial t} v(t, x) + \frac{\partial}{\partial x} \frac{v^2(t, x)}{2} \right) dt = \frac{0.77\nu \int \frac{\partial^2}{\partial x^2} v(t, x) dt}{\pi}$$

$$0.73tv(0, x) = 0.73tv_0(x)$$

- Explanation: We replace  $u$  with  $v$  and  $\partial_t$  with  $\frac{\partial}{\partial t}$ . We integrate and multiply some factors on both sides of the equation at the same time.

### F.2.2 Advection

- Original form:

$$\begin{aligned}\partial_t u(t, x) + \beta \partial_x u(t, x) &= 0, \quad x \in (0, 1), t \in (0, 2], \\ u(0, x) &= u_0(x), \quad x \in (0, 1),\end{aligned}$$

- After augmented:

$$\begin{aligned}1.45 \int \left( c \frac{\partial}{\partial x} A(t, x) + \frac{\partial}{\partial t} A(t, x) \right) dt &= 0 \\ A(0, x) &= A_0(x)\end{aligned}$$

- Explanation: We replace  $u$  with  $A$ ,  $\partial_t, \partial_x$  with  $\frac{\partial}{\partial t}, \frac{\partial}{\partial x}$ , and  $\beta$  with  $c$ . We integrate and multiply some factors on both sides of the equation at the same time.

### F.2.3 CFD-1D

- Original form:

$$\begin{aligned}\partial_t \rho + \nabla \cdot (\rho \mathbf{v}) &= 0, \\ \rho(\partial_t \mathbf{v} + \mathbf{v} \cdot \nabla \mathbf{v}) &= -\nabla p + \eta \Delta \mathbf{v} + (\zeta + \eta/3) \nabla(\nabla \cdot \mathbf{v}), \\ \partial_t \left[ \epsilon + \frac{\rho v^2}{2} \right] + \nabla \cdot \left[ \left( \epsilon + p + \frac{\rho v^2}{2} \right) \mathbf{v} - \mathbf{v} \cdot \sigma' \right] &= 0,\end{aligned}$$

- After augmented:

$$\varrho(t, x) \frac{\partial}{\partial x} \mathbf{w}(t, x) + \frac{\partial}{\partial t} \varrho(t, x) = 0 \tag{10}$$

$$\begin{aligned}0.61 \left( \mathbf{w}(t, x) \frac{\partial}{\partial x} \mathbf{w}(t, x) + \frac{\partial}{\partial t} \mathbf{w}(t, x) \right) \varrho(t, x) &= \\ 0.61 \eta \frac{\partial^2}{\partial x^2} \mathbf{w}(t, x) + 0.61 \left( \chi + \frac{\eta}{3} \right) \frac{\partial^2}{\partial x^2} \mathbf{w}(t, x) - 0.61 \frac{\partial}{\partial x} p(t, x) &\tag{11}\end{aligned}$$

- Explanation: We replaced many symbols, such as replacing  $\nabla$  with  $\partial_t$  and  $\Delta$  with  $\frac{\partial^2}{\partial x^2}$ . We integrate and multiply some factors on both sides of the equation at the same time. We also swapped the order of some items, such as  $\zeta + \eta/3$ .

Table 9: Detailed Data Information: The total amounts of training data, sampled training data, total validation data, and sampled validation data are presented as lists. These lists correspond to 1D, 2D, and 3D data respectively.

Dims	Total training	Sampled training	Total validation	Sampled Validation
1D	218T	378K	269M	42K
2D	3.13T	42K	38M	5K
3D	748K	0.63K	9K	0.07K

### F.3 Pre-training process of PDE-Aligner

In our architecture, the PDE-Aligner is divided into two components: a text encoder and a physics encoder. The text encoder utilizes the pre-trained albert-math model [28], which is highly capable of processing LaTeX-encoded PDE captions due to its extensive training on a large corpus of LaTeX data. For the physics encoder, we employ the pre-trained Fourier encoder from OmniArch, known for its strong ability to capture physical field features. We adopt a large-batch contrastive learning approach similar to SimCLR [4]. The training involves a stochastic sampling strategy with an equal probability (50%) of selecting either canonical PDE captions sourced directly from textbooks or augmented PDE captions. The latter is assumed to enhance the text encoder’s generalization capabilities while

Table 10: Detailed Hyper-parameters Settings: The init learning rate, optimizer, scheduler, hidden size, trainable params, total params, steps, and GPU hrs are presented as lists.

Hyper-parameters	Value
<b>Init Learning Rate</b>	1e-4
<b>Optimizer</b>	Adam
<b>Scheduler</b>	Cosine Annealing
<b>Hidden Size</b>	768
<b>Trainable Params</b>	1.2M
<b>Total Params</b>	195M
<b>Steps</b>	37k
<b>GPU hrs</b>	75

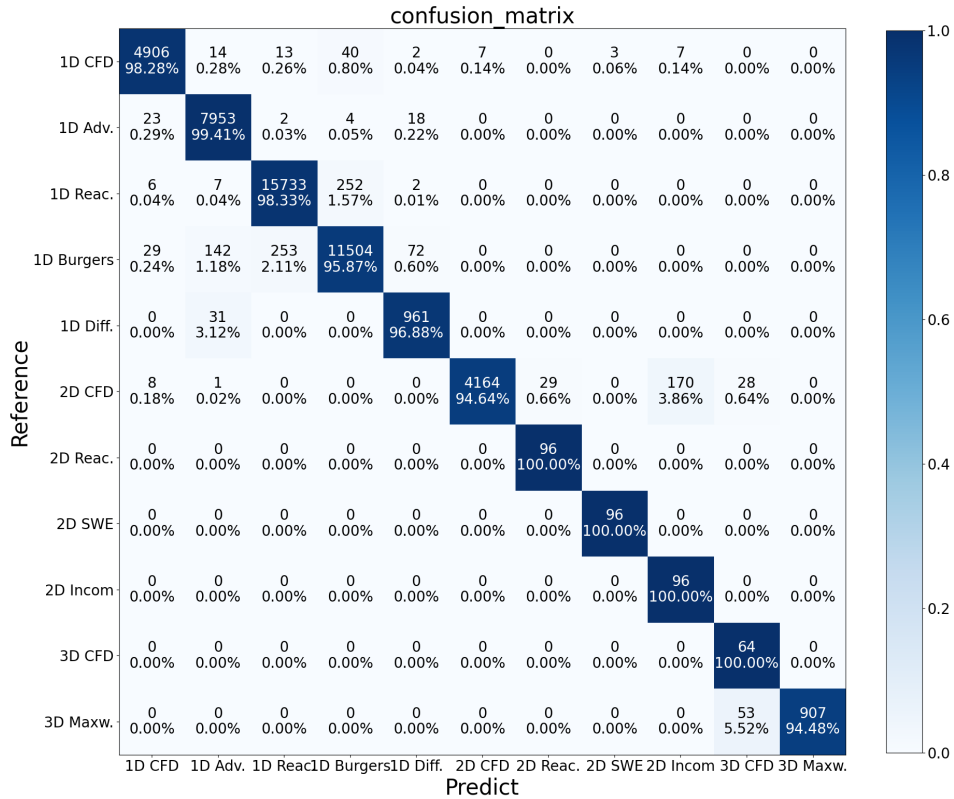


Figure 8: **The confusion matrix of the PDE-Aligner classification results.** PDE-Aligner can perceive physical field categories based on equation text information and physical field features, and the classification accuracy rate exceeds 0.94 on all ten categories.

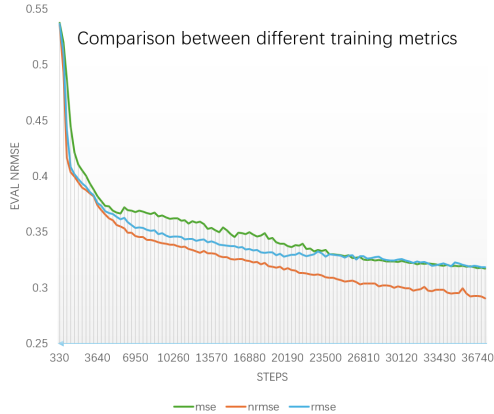


Figure 9: The training loss curve using different metrics.

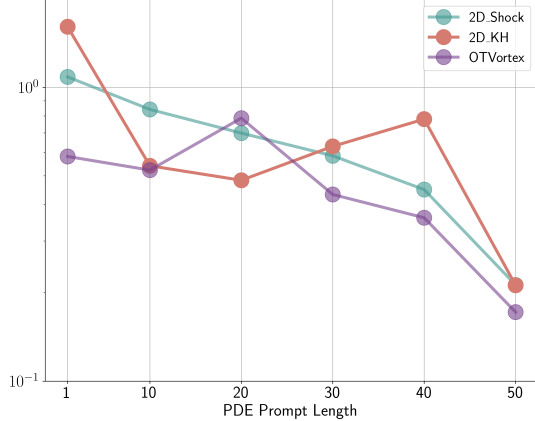


Figure 10: Zero-shot learning nRMSE for T+1 timesteps with varying context lengths.

retaining critical PDE information in textual form. The weights of the text encoder and physics encoder are fixed during the PDE-Aligner training process. The training data details for PDE-Aligner are shown in Table 9, and the hyperparameter settings are provided in Table 10.

During the fine-tuning phase, the PDE-Aligner evaluates the alignment of gold-standard PDE captions with the state of physical fields at each step of generator G’s decoding process. The resulting rewards are averaged over the temporal dimension and finalized upon the completion of inference. The intuition behind the PDE-Aligner fine-tuning is to help OmniArch distinguish the patterns behind different PDE systems. To verify the PDE-Aligner’s ability to perceive physical information, we equipped it with a classification head to classify physical fields. The results, shown in Figure 8, indicate that the PDE-Aligner effectively aligns with physical laws.

## G Further ablation study

We have conducted an ablation study on batch-wise nRMSE. We use nRMSE, RMSE, and MSE respectively as loss functions in the training process. We found that nRMSE leads to a more unified loss scale for different PDEs, benefiting OmniArch’s convergence. Table 11 shows nRMSE yielded lower training losses compared to MSE and RMSE (up to 9.3% improvement). While we did encounter gradient calculation issues in extreme cases, these were mitigated by adding a small  $\epsilon$  to the squared norm of the true labels (averaged over the spatial dimension). Utilizing nRMSE as a training loss function aims to simultaneously reduce all channels, irrespective of their relative numerical values. The loss curve is shown in Figure 9.

Table 11: Training loss metrics ablation study.

Steps	MSE	RMSE	nRMSE
10K	0.3624	0.3458	<b>0.3386</b> (-2.08%)
20K	0.3371	0.3289	<b>0.3175</b> (-3.47%)
30K	0.3240	0.3225	<b>0.3005</b> (-6.82%)
40K	0.3181	0.3183	<b>0.2887</b> (-9.83%)

## H More results

### H.1 Zero-shot Learning Capability

Our examination of 2D PDE predictions reveals that, in contrast to task-tuned models, the OmniArch model adeptly captures both low- and high-frequency patterns in in-domain PDEs such as Reaction

Diffusion, CFD, Shallow Water, and Incompressible NS. Task-tuned models often miss key features, occasionally leading to erroneous representations of the primary physics. For out-of-domain PDEs, delineated by a red-dotted box in the figure, we evaluated the models’ ability to predict unseen PDEs without fine-tuning or parameter adjustment. While task-tuned models consistently failed at this zero-shot learning task, OmniArch successfully predicted essential low-frequency background patterns, though it struggled with high-frequency details. Details on the zero-shot dataset, including shock wave, Kelvin-Helmholtz (KH), and Orszag-Tang Vortex (OTVortex) phenomena, are provided in Appendix C.2.

In our zero-shot learning evaluation, we explore the minimum number of time steps necessary to formulate accurate neural operators. We also probe the OmniArch model’s ability to generalize to new physics scenarios without parameter adjustments. As indicated in Table 2 and Figure 10, a longer temporal context typically enhances model performance, resulting in lower nRMSE scores across tasks. Notably, our model exhibits impressive zero-shot learning capabilities, maintaining robustness against mesh and temporal interpolation variations, even with fewer than 20 time steps of context.

## H.2 Dynamic Prompt Length for Efficient Inference

We examine the trade-off between inference speed and accuracy using dynamic prompt lengths in our model. The goal is to determine whether shorter prompts can accelerate inference times on the CPU without significantly sacrificing precision.

Our approach varies the prompt length from 2 tokens (derived from a 50 time step interval) to 100 tokens (from a 1 time step interval) to predict physical fields at  $u_{101}$ . As shown in Figure 7, longer prompts yield higher precision with less variance, while shorter prompts can expedite inference by up to 10 times compared to full-length prompts. In particular, our model demonstrates an inherent ability to learn temporal differences from the input sequence, negating the need for explicit time-step inputs.

## H.3 Fine-tuned for Inverse Problems

Demonstrating a model’s capability to infer hidden physical parameters from known equations is a critical test of its ability to learn underlying physics. Following the methodology of MPP [17], we evaluate our model on two inverse problems for incompressible Navier-Stokes equations: 1) Forcing Identification, and 2) Buoyancy Determination.

Table 12: RMSE for Parameter Estimation in Inverse Problems.

Methods	Forcing	Buoyancy
<b>MPP</b>	$0.2 \pm 0.008$	$0.78 \pm 0.006$
<b>OmniArch</b>	$0.16 \pm 0.005$	$0.73 \pm 0.012$
<b>Scratch</b>	$0.39 \pm 0.012$	$0.83 \pm 0.027$

The results in Table 12 demonstrate that OmniArch outperforms MPP in parameter estimation tasks, with lower RMSE values indicating more accurate predictions. Models trained from scratch yield the highest errors, underscoring the effectiveness of our fine-tuning approach. This evidence supports the notion that OmniArch is not only proficient in forward simulations but also exhibits superior performance in deducing hidden dynamics within complex systems.

## H.4 Rollout Predictions

We perform rollout experiments to compare the performance of the Fourier Neural Operator (FNO) model and our proposed OmniArch model, as depicted in Figure 11, 12, 13, 14. Our findings indicate that OmniArch demonstrates superior adherence to the underlying physics laws in the initial timesteps, as opposed to merely replicating patterns from other trajectories. This improved fidelity is likely a result of fine-tuning with PDE-Aligner, which isolates the model from the influences of alternate PDE systems, thereby enhancing the model’s ability to generalize physical dynamics.

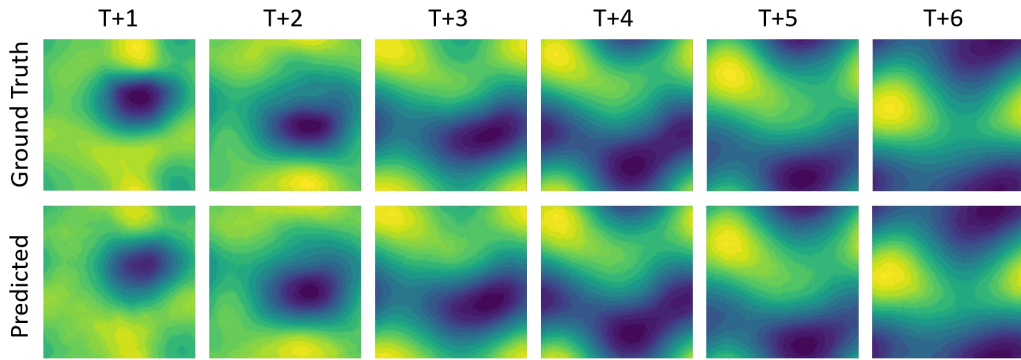


Figure 11: Prediction results of OmniArch on CFD-2D dataset. Displaying time steps T+1 to T+6, the top row shows ground truth data, and the bottom row illustrates OmniArch's predictions.

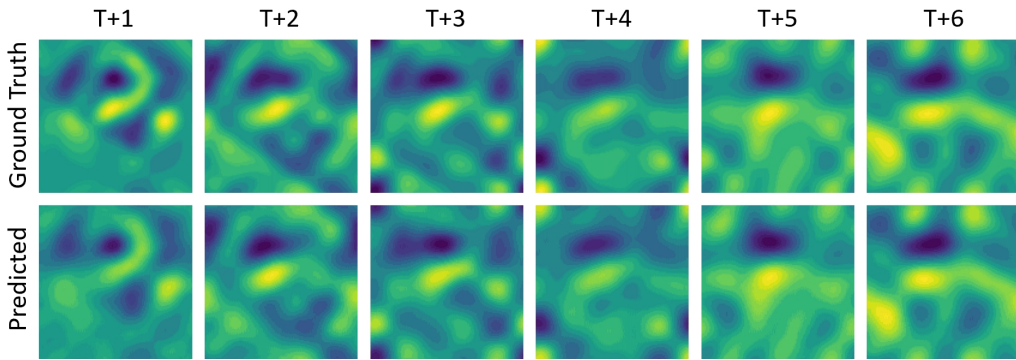


Figure 12: Prediction results of OmniArch on CFD-2D dataset. Displaying time steps T+1 to T+6, the top row shows ground truth data, and the bottom row illustrates OmniArch's predictions.

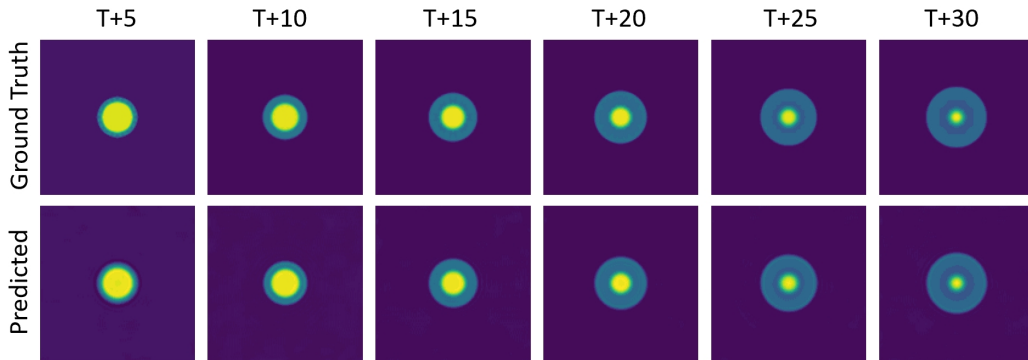


Figure 13: Prediction results of OmniArch on SWE dataset. Displaying time steps T+5 to T+30, the top row shows ground truth data, and the bottom row illustrates OmniArch's predictions.

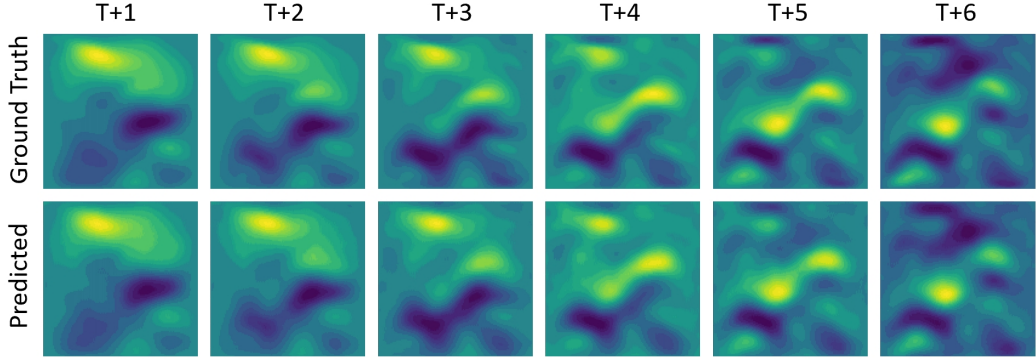


Figure 14: Prediction results of OmniArch on Incom dataset. Displaying time steps T+1 to T+6, the top row shows ground truth data, and the bottom row illustrates OmniArch’s predictions.

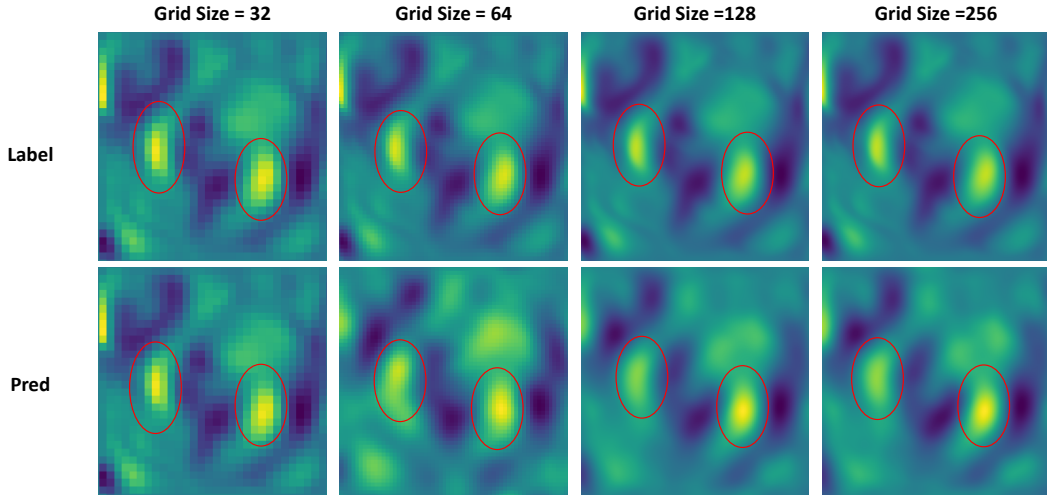


Figure 15: Multi-scale results of OmniArch-Large with different grid sizes.

### H.5 Multi-scale Inference Results

To thoroughly evaluate the multi-scale forecasting capabilities of OmniArch, extensive experiments were conducted across four different grid resolutions:  $32 \times 32$ ,  $64 \times 64$ ,  $128 \times 128$ , and  $256 \times 256$ . Figure 15 presents the visualization results at  $T + 50$  time step on the Incom dataset. These results demonstrate OmniArch’s robust ability to accurately capture local patterns across varying grid sizes, confirming its effectiveness in handling multi-scale data without losing detail or accuracy.

### H.6 More results in different problem settings

We tested our model on CFD-2D problems under various settings of the Navier-Stokes equations to evaluate its performance across different scenarios. The goal was to determine the robustness and adaptability of our model, OmniArch, compared to other state-of-the-art models like MPP, FNO, and U-Net.

Table 13 summarizes the performance results of our model, OmniArch (FT), against MPP (FT), FNO, and U-Net across multiple problem settings. These settings include variations in Mach number ( $M$ ), viscosity ( $\eta$ ), and diffusivity ( $\xi$ ), both in inviscid and turbulent conditions with random periodic boundary conditions.

These results consistently show that OmniArch performs better across various settings, demonstrating its robustness and effectiveness. The performance advantage of OmniArch is evident across different

Table 13: The different problem settings in 2D Navier Stokes equation performance.

Problem Settings	OmniArch(FT)	MPP(FT)	FNO	U-Net
$M = 0.1$ , inviscid Rand periodic	<b>0.1600</b>	0.5866	0.38	0.66
$M = 0.1, \eta = \xi = 0.01$ Rand periodic	<b>0.1215</b>	0.5286	0.17	0.71
$M = 0.1, \eta = \xi = 0.1$ Rand periodic	<b>0.0273</b>	0.5761	0.36	5.1
$M = 1.0, \eta = \xi = 0.01$ Rand periodic	<b>0.1301</b>	0.5096	0.196	0.36
$M = 1.0$ , inviscid Rand periodic	<b>0.1387</b>	0.5391	0.35	0.47
$M = 1.0, \eta = \xi = 0.1$ Rand periodic	<b>0.0308</b>	0.5033	0.098	0.92
$M = 0.1$ , inviscid Turb periodic	<b>0.2219</b>	0.3949	0.16	0.19
$M = 1.0$ , inviscid Turb periodic	<b>0.1624</b>	0.5412	0.43	0.14

Mach numbers, viscosity, and diffusivity settings, both in inviscid and turbulent conditions. These findings highlight the model’s capability to generalize and maintain high accuracy in diverse and challenging CFD scenarios.

### H.7 GPU Memory Usage and Inference Time

We also report the runtime and memory usage in Table 14. OmniArch consistently uses less GPU memory than MPP across all model sizes, demonstrating its efficiency in resource utilization. While FNO and U-Net have lower GPU memory usage and faster inference times, OmniArch’s performance remains competitive, particularly considering its ability to handle a wider range of PDE tasks across 1D, 2D, and 3D domains.

Table 14: The runtime and memory usage between different models.

Model	Size	GPU Memory	Inference Time
<b>OmniArch</b>	Tiny	671MB	0.0125s
	Small	866MB	0.0129s
	Base	1591MB	0.0136s
	Large	3109MB	0.0248s
<b>MPP</b>	Tiny	1378MB	0.0387s
	Small	1532MB	0.0390s
	Base	1620MB	0.0391s
	Large	3270MB	0.0831s
<b>FNO</b>	-	690MB	0.0018s
<b>U-Net</b>	-	830MB	0.0027s

## NeurIPS Paper Checklist

### 1. Claims

Question: Do the main claims made in the abstract and introduction accurately reflect the paper's contributions and scope?

Answer: [Yes]

Justification: The motivation and contribution are shown in the introduction, and the results match the claim.

Guidelines:

- The answer NA means that the abstract and introduction do not include the claims made in the paper.
- The abstract and/or introduction should clearly state the claims made, including the contributions made in the paper and important assumptions and limitations. A No or NA answer to this question will not be perceived well by the reviewers.
- The claims made should match theoretical and experimental results, and reflect how much the results can be expected to generalize to other settings.
- It is fine to include aspirational goals as motivation as long as it is clear that these goals are not attained by the paper.

### 2. Limitations

Question: Does the paper discuss the limitations of the work performed by the authors?

Answer: [Yes]

Justification: The limitations is discussed in section B.

Guidelines:

- The answer NA means that the paper has no limitation while the answer No means that the paper has limitations, but those are not discussed in the paper.
- The authors are encouraged to create a separate "Limitations" section in their paper.
- The paper should point out any strong assumptions and how robust the results are to violations of these assumptions (e.g., independence assumptions, noiseless settings, model well-specification, asymptotic approximations only holding locally). The authors should reflect on how these assumptions might be violated in practice and what the implications would be.
- The authors should reflect on the scope of the claims made, e.g., if the approach was only tested on a few datasets or with a few runs. In general, empirical results often depend on implicit assumptions, which should be articulated.
- The authors should reflect on the factors that influence the performance of the approach. For example, a facial recognition algorithm may perform poorly when the image resolution is low or images are taken in low lighting. Or a speech-to-text system might not be used reliably to provide closed captions for online lectures because it fails to handle technical jargon.
- The authors should discuss the computational efficiency of the proposed algorithms and how they scale with dataset size.
- If applicable, the authors should discuss possible limitations of their approach to addressing problems of privacy and fairness.
- While the authors might fear that complete honesty about limitations might be used by reviewers as grounds for rejection, a worse outcome might be that reviewers discover limitations that aren't acknowledged in the paper. The authors should use their best judgment and recognize that individual actions in favor of transparency play an important role in developing norms that preserve the integrity of the community. Reviewers will be specifically instructed to not penalize honesty concerning limitations.

### 3. Theory Assumptions and Proofs

Question: For each theoretical result, does the paper provide the full set of assumptions and a complete (and correct) proof?

Answer: [Yes]

Justification: In the design of OmniArch(see section 3.1), we provide theoretical analysis.

Guidelines:

- The answer NA means that the paper does not include theoretical results.
- All the theorems, formulas, and proofs in the paper should be numbered and cross-referenced.
- All assumptions should be clearly stated or referenced in the statement of any theorems.
- The proofs can either appear in the main paper or the supplemental material, but if they appear in the supplemental material, the authors are encouraged to provide a short proof sketch to provide intuition.
- Inversely, any informal proof provided in the core of the paper should be complemented by formal proofs provided in the appendix or supplemental material.
- Theorems and Lemmas that the proof relies upon should be properly referenced.

#### 4. Experimental Result Reproducibility

Question: Does the paper fully disclose all the information needed to reproduce the main experimental results of the paper to the extent that it affects the main claims and/or conclusions of the paper (regardless of whether the code and data are provided or not)?

Answer: [Yes]

Justification: We include very detailed experiment setup C, data cook receipts and the training detailsE in appendix. Also, we provide the code in the supplementary files.

Guidelines:

- The answer NA means that the paper does not include experiments.
- If the paper includes experiments, a No answer to this question will not be perceived well by the reviewers: Making the paper reproducible is important, regardless of whether the code and data are provided or not.
- If the contribution is a dataset and/or model, the authors should describe the steps taken to make their results reproducible or verifiable.
- Depending on the contribution, reproducibility can be accomplished in various ways. For example, if the contribution is a novel architecture, describing the architecture fully might suffice, or if the contribution is a specific model and empirical evaluation, it may be necessary to either make it possible for others to replicate the model with the same dataset, or provide access to the model. In general, releasing code and data is often one good way to accomplish this, but reproducibility can also be provided via detailed instructions for how to replicate the results, access to a hosted model (e.g., in the case of a large language model), releasing of a model checkpoint, or other means that are appropriate to the research performed.
- While NeurIPS does not require releasing code, the conference does require all submissions to provide some reasonable avenue for reproducibility, which may depend on the nature of the contribution. For example
  - (a) If the contribution is primarily a new algorithm, the paper should make it clear how to reproduce that algorithm.
  - (b) If the contribution is primarily a new model architecture, the paper should describe the architecture clearly and fully.
  - (c) If the contribution is a new model (e.g., a large language model), then there should either be a way to access this model for reproducing the results or a way to reproduce the model (e.g., with an open-source dataset or instructions for how to construct the dataset).
  - (d) We recognize that reproducibility may be tricky in some cases, in which case authors are welcome to describe the particular way they provide for reproducibility. In the case of closed-source models, it may be that access to the model is limited in some way (e.g., to registered users), but it should be possible for other researchers to have some path to reproducing or verifying the results.

#### 5. Open access to data and code

Question: Does the paper provide open access to the data and code, with sufficient instructions to faithfully reproduce the main experimental results, as described in supplemental material?

Answer: [Yes]

Justification: We provide full code and running scripts in the supplementary. The data we used include PDEBench(<https://github.com/pdebench/PDEBench>) and PDEArena(<https://pdearena.github.io/pdearena/>) are all open-sourced.

Guidelines:

- The answer NA means that the paper does not include experiments requiring code.
- Please see the NeurIPS code and data submission guidelines (<https://nips.cc/public/guides/CodeSubmissionPolicy>) for more details.
- While we encourage the release of code and data, we understand that this might not be possible, so “No” is an acceptable answer. Papers cannot be rejected simply for not including code, unless this is central to the contribution (e.g., for a new open-source benchmark).
- The instructions should contain the exact command and environment needed to run to reproduce the results. See the NeurIPS code and data submission guidelines (<https://nips.cc/public/guides/CodeSubmissionPolicy>) for more details.
- The authors should provide instructions on data access and preparation, including how to access the raw data, preprocessed data, intermediate data, generated data, etc.
- The authors should provide scripts to reproduce all experimental results for the new proposed method and baselines. If only a subset of experiments are reproducible, they should state which ones are omitted from the script and why.
- At submission time, to preserve anonymity, the authors should release anonymized versions (if applicable).
- Providing as much information as possible in supplemental material (appended to the paper) is recommended, but including URLs to data and code is permitted.

## 6. Experimental Setting/Details

Question: Does the paper specify all the training and test details (e.g., data splits, hyper-parameters, how they were chosen, type of optimizer, etc.) necessary to understand the results?

Answer: [Yes]

Justification: We provide the details of data preparation, baselines, software/hardware settings, metrics, and other details in section 4 and appendix C, appendix E.

Guidelines:

- The answer NA means that the paper does not include experiments.
- The experimental setting should be presented in the core of the paper to a level of detail that is necessary to appreciate the results and make sense of them.
- The full details can be provided either with the code, in the appendix, or as supplemental material.

## 7. Experiment Statistical Significance

Question: Does the paper report error bars suitably and correctly defined or other appropriate information about the statistical significance of the experiments?

Answer: [Yes]

Justification: We use the average performance of repeated experiments in the main results, and show the standard deviation.

Guidelines:

- The answer NA means that the paper does not include experiments.
- The authors should answer "Yes" if the results are accompanied by error bars, confidence intervals, or statistical significance tests, at least for the experiments that support the main claims of the paper.
- The factors of variability that the error bars are capturing should be clearly stated (for example, train/test split, initialization, random drawing of some parameter, or overall run with given experimental conditions).

- The method for calculating the error bars should be explained (closed form formula, call to a library function, bootstrap, etc.)
- The assumptions made should be given (e.g., Normally distributed errors).
- It should be clear whether the error bar is the standard deviation or the standard error of the mean.
- It is OK to report 1-sigma error bars, but one should state it. The authors should preferably report a 2-sigma error bar and then state that they have a 96% CI if the hypothesis of Normality of errors is not verified.
- For asymmetric distributions, the authors should be careful not to show in tables or figures symmetric error bars that would yield results that are out of range (e.g. negative error rates).
- If error bars are reported in tables or plots, The authors should explain in the text how they were calculated and reference the corresponding figures or tables in the text.

## 8. Experiments Compute Resources

Question: For each experiment, does the paper provide sufficient information on the computer resources (type of compute workers, memory, time of execution) needed to reproduce the experiments?

Answer: [Yes]

Justification: We include our hardware resources and training details in the Appendix E.

Guidelines:

- The answer NA means that the paper does not include experiments.
- The paper should indicate the type of compute workers CPU or GPU, internal cluster, or cloud provider, including relevant memory and storage.
- The paper should provide the amount of compute required for each of the individual experimental runs as well as estimate the total compute.
- The paper should disclose whether the full research project required more compute than the experiments reported in the paper (e.g., preliminary or failed experiments that didn't make it into the paper).

## 9. Code Of Ethics

Question: Does the research conducted in the paper conform, in every respect, with the NeurIPS Code of Ethics <https://neurips.cc/public/EthicsGuidelines>?

Answer: [Yes]

Justification: We use the correct and broad domain conflicts to preserve anonymity.

Guidelines:

- The answer NA means that the authors have not reviewed the NeurIPS Code of Ethics.
- If the authors answer No, they should explain the special circumstances that require a deviation from the Code of Ethics.
- The authors should make sure to preserve anonymity (e.g., if there is a special consideration due to laws or regulations in their jurisdiction).

## 10. Broader Impacts

Question: Does the paper discuss both potential positive societal impacts and negative societal impacts of the work performed?

Answer: [NA]

Justification: There is no societal impact of the work performed.

Guidelines:

- The answer NA means that there is no societal impact of the work performed.
- If the authors answer NA or No, they should explain why their work has no societal impact or why the paper does not address societal impact.
- Examples of negative societal impacts include potential malicious or unintended uses (e.g., disinformation, generating fake profiles, surveillance), fairness considerations (e.g., deployment of technologies that could make decisions that unfairly impact specific groups), privacy considerations, and security considerations.

- The conference expects that many papers will be foundational research and not tied to particular applications, let alone deployments. However, if there is a direct path to any negative applications, the authors should point it out. For example, it is legitimate to point out that an improvement in the quality of generative models could be used to generate deepfakes for disinformation. On the other hand, it is not needed to point out that a generic algorithm for optimizing neural networks could enable people to train models that generate Deepfakes faster.
- The authors should consider possible harms that could arise when the technology is being used as intended and functioning correctly harms that could arise when the technology is being used as intended but gives incorrect results, and harms following from (intentional or unintentional) misuse of the technology.
- If there are negative societal impacts, the authors could also discuss possible mitigation strategies (e.g., gated release of models, providing defenses in addition to attacks, mechanisms for monitoring misuse, mechanisms to monitor how a system learns from feedback over time, improving the efficiency and accessibility of ML).

## 11. Safeguards

Question: Does the paper describe safeguards that have been put in place for the responsible release of data or models that have a high risk for misuse (e.g., pre-trained language models, image generators, or scraped datasets)?

Answer: [NA]

Justification: The paper does not have such risks.

Guidelines:

- The answer NA means that the paper poses no such risks.
- Released models that have a high risk for misuse or dual-use should be released with necessary safeguards to allow for controlled use of the model, for example by requiring that users adhere to usage guidelines or restrictions to access the model or implementing safety filters.
- Datasets that have been scraped from the Internet could pose safety risks. The authors should describe how they avoided releasing unsafe images.
- We recognize that providing effective safeguards is challenging, and many papers do not require this, but we encourage authors to take this into account and make the best faith effort.

## 12. Licenses for existing assets

Question: Are the creators or original owners of assets (e.g., code, data, models), used in the paper, properly credited, and are the license and terms of use explicitly mentioned and properly respected?

Answer: [Yes]

Justification: The dataset and models we used in 4 is properly cited.

Guidelines:

- The answer NA means that the paper does not use existing assets.
- The authors should cite the original paper that produced the code package or dataset.
- The authors should state which version of the asset is used and, if possible, include a URL.
- The name of the license (e.g., CC-BY 4.0) should be included for each asset.
- For scraped data from a particular source (e.g., website), the copyright and terms of service of that source should be provided.
- If assets are released, the license, copyright information, and terms of use in the package should be provided. For popular datasets, [paperswithcode.com/datasets](https://paperswithcode.com/datasets) has curated licenses for some datasets. Their licensing guide can help determine the license of a dataset.
- For existing datasets that are re-packaged, both the original license and the license of the derived asset (if it has changed) should be provided.

- If this information is not available online, the authors are encouraged to reach out to the asset’s creators.

### 13. **New Assets**

Question: Are new assets introduced in the paper well documented and is the documentation provided alongside the assets?

Answer: [Yes]

Justification: We have included the correct license in the supplementary.

Guidelines:

- The answer NA means that the paper does not release new assets.
- Researchers should communicate the details of the dataset/code/model as part of their submissions via structured templates. This includes details about training, license, limitations, etc.
- The paper should discuss whether and how consent was obtained from people whose asset is used.
- At submission time, remember to anonymize your assets (if applicable). You can either create an anonymized URL or include an anonymized zip file.

### 14. **Crowdsourcing and Research with Human Subjects**

Question: For crowdsourcing experiments and research with human subjects, does the paper include the full text of instructions given to participants and screenshots, if applicable, as well as details about compensation (if any)?

Answer: [NA]

Justification: The paper does not involve crowdsourcing or research with human subjects.

Guidelines:

- The answer NA means that the paper does not involve crowdsourcing nor research with human subjects.
- Including this information in the supplemental material is fine, but if the main contribution of the paper involves human subjects, then as much detail as possible should be included in the main paper.
- According to the NeurIPS Code of Ethics, workers involved in data collection, curation, or other labor should be paid at least the minimum wage in the country of the data collector.

### 15. **Institutional Review Board (IRB) Approvals or Equivalent for Research with Human Subjects**

Question: Does the paper describe potential risks incurred by study participants, whether such risks were disclosed to the subjects, and whether Institutional Review Board (IRB) approvals (or an equivalent approval/review based on the requirements of your country or institution) were obtained?

Answer: [NA]

Justification: The paper does not involve crowdsourcing nor research with human subjects.

Guidelines:

- The answer NA means that the paper does not involve crowdsourcing nor research with human subjects.
- Depending on the country in which research is conducted, IRB approval (or equivalent) may be required for any human subjects research. If you obtained IRB approval, you should clearly state this in the paper.
- We recognize that the procedures for this may vary significantly between institutions and locations, and we expect authors to adhere to the NeurIPS Code of Ethics and the guidelines for their institution.
- For initial submissions, do not include any information that would break anonymity (if applicable), such as the institution conducting the review.